# The application of plasma assisted chemical vapour deposition of ZrC onto a Zr-alloy substrate

**A Sunil**

**22667660**

Dissertation submitted in partial fulfilment of the requirements for the degree Master of Engineering in a Nuclear Engineering the Potchefstroom Campus of the North-West University

Supervisor: Prof J Markgraaff

October 2017

# ABSTRACT

Zirconium alloys are widely used as fuel cladding materials in Light Water Reactors (LWR) due to their excellent mechanical properties and low neutron absorption. The incident that occurred at Japan's Fukushima Daiichi nuclear power plant was aggravated by the lack of resistance of the zirconium alloy, as fuel rod cladding exposed to steam oxidation produces explosive hydrogen. Thus, the improvement against oxidation of Zr alloy fuel cladding by coatings, such as, silicon carbide (SiC) and zirconium carbide (ZrC) has become an area of interest. This study investigated available literature on the deposition of ZrC using various coating methods in order to find and apply a feasible method to apply ZrC that is cost effective. This study applied a Radio Frequency cold plasma assisted chemical vapour deposition method using a set of parameters, in an effort to coat ZrC on a mild steel substrate (instead of Zr alloy substrate) followed by the use of Scanning Electron Microscopy (SEM) and X-ray Diffraction (XRD) to characterise the coated product. The results obtained showed that a sufficient ZrC layer was not deposited on the substrates. This is attributed to inadequate vacuum and or the leak of oxygen to the reactor. Further studies using a different range of parameters of the cold plasma chemical vapour deposition method used is recommended to improve on the deposition characteristics and determination of the feasibility of ZrC coating on Zr alloy fuel cladding materials.

**Keywords:** Light Water Reactors (LWR), Nuclear energy, Zirconium alloys, Zirconium Carbide, Substrate, Coating, Cold plasma assisted chemical vapour deposition

# ACKNOWLEDGEMENTS

I would like to thank my study leader, Prof. Johann Markgraaff for all his extremely valuable inputs during this study. I am grateful for your support.

My sincere gratitude to Dr Hertzog Bissett, Dr Johan Nel and Dr Jaco Van der Walt for their time and invaluable support during the experimental phase of this project and access to The South African Nuclear Energy Corporation (NECSA) facilities.

I would also like to thank Eskom, Integrated Plant Design-Fleet (IPD-F), for giving me the opportunity to study part-time and for funding my studies.

Finally, I would like to thank my wife, Dr Manjusha Sunil for her continuous love, support, assistance and encouragement.

# TABLE OF CONTENTS

# LIST OF FIGURES

# LIST OF TABLES

# LIST OF ABBREVIATIONS

| | |
|---|---|
| bcc | Body Centred Cubic |
| fcc | Face Centred Cubic |
| hcp | Hexagonal Close Packed |
| ICDD | International Centre for Diffraction Data |
| JCPDS | Joint Committee on Powder Diffraction Standards |
| LWR | Light Water Reactor |
| SEM | Scanning Electron Microscopy |
| XRD | X-ray Diffraction |
| XPS | X-ray Photoelectron Spectroscopy |
| PWR | Pressurised Water Reactor |
| CVD | Chemical Vapour Deposition |
| PVD | Physical Vapour Deposition |
| EB-PVD | Electron Beam Physical Vapour Deposition |
| PLD | Pulsed Laser Deposition |
| RMI | Reactive Melt Infiltration |
| APS | Atmospheric Plasma Spraying |
| VPS | Vacuum Plasma Spray |
| PS | Plasma Spraying |
| DC | Direct Current |
| RF | Radio-Frequency |
| LPPS | Low Pressure Plasma Spray |
| PS-PVD | Plasma Spray- Physical Vapour Deposition |
| LPPS-TF | Low Pressure Plasma Spray-Thin Film |

# Chapter 1

# Introduction

## 1.1 Introduction

Generation III (Gen III) Light Water Reactors (LWRs) presently dominate the commercial implementation of nuclear energy and will probably continue to do so for at least this century and possibly for much longer. Several countries are building and/or have plans to build more LWRs in the near future [1].

Zirconium alloys are widely used as fuel cladding materials in LWRs due to their excellent mechanical properties, as well as their low neutron absorption [1] [2]. However, oxidation is one of the key life-limiting phenomena of zirconium cladding.

The Fukushima accident demonstrated how an earthquake and floods due to tsunami can combine and lead to prolonged power loss and the total loss of the heat sink of the reactor. During this misfortune, the accident was aggravated by hydrogen explosions due to the fact that hydrogen was produced by the reaction between zirconium alloy cladding material and steam at high temperature. The high temperature was formed due to cooling water pump failure as a result of sea water ingress into electrical transformer housings, which shows the vulnerability of zirconium alloy as cladding material under such conditions.

In order to mitigate the problems of oxidation and hydrogen production of zirconium alloys at high temperatures, new methods of improving cladding materials are being investigated. The improvement against oxidation of Zr alloy fuel cladding, by coatings, such as, silicon carbide (SiC) and zirconium carbide (ZrC), has become an important topic [3].

Due to the excellent properties of ZrC, it has been used as a coating material in many demanding applications where the role of the microstructure and composition of the deposited films are critical [3].

## 1.2 Problem statement

Thin film deposition techniques have drawbacks of high operating cost and low deposition rates that strongly restrict their application ranges. The currently used coating techniques of ZrC experiences problems of wettability and non-uniform thickness of coating on cladding materials and does not always ensure stoichiometric carbon to zirconium ratios in the final ZrC coated product.

## 1.3 Aim

The aim of this study is to review the literature of the deposition of ZrC using different coating methods in an effort to find and apply a feasible method to deposit ZrC on zirconium alloy nuclear fuel rods and in an effort to overcome the non-stoichiometric coating development. Also, to review Zr alloy as fuel rod material to better understand material interface interactions on application of ZrC as a coating material on fuel rods.

## 1.4 Methodology

The methodology used is described as follows:

- Literature review of the deposition of ZrC using different coating methods
- Identification of the most feasible method to deposit ZrC on zirconium alloy nuclear fuel rods
- Experimental work
- Verification of the results
- Conclusion and recommendations

## 1.5 Dissertation Structure

This dissertation is structured as follows:

**Chapter 1** contains introduction, problem statement, aim, methodology and dissertation structure.

**Chapter 2** consists of properties, phase chemistry and composition of ZrC and its oxidation. This chapter also provides a literature review of the deposition of ZrC using different coating methods.

**Chapter 3** describes the experimental setup, stoichiometry, temperature calibration of the reactor, substrate description and experimental procedure.

**Chapter 4** presents the Scanning Electron Microscope (SEM) and X-ray Diffraction (XRD) results of the coated samples and the verification and discussion of the results.

**Chapter 5** provides conclusions and recommendations reached in the dissertation.

# Chapter 2

# Literature Review

## 2.1 Properties of ZrC

Zirconium carbide (ZrC) is one of the hardest compounds with a micro-hardness value of ~2600 kg/mm$^2$. Due to this property, ZrC has been used to produce cutting tools and wear-resistant coatings. It is also an ideal material for ultra-high temperature applications, due to its high melting point, solid-state phase stability and good thermo-mechanical and thermochemical properties. In addition to its high degree of hardness and high melting temperature, ZrC displays a high emissivity and high electric capacity at elevated temperatures. Thus, ZrC is a favourable material for use in thermo-photovoltaic radiators and field emitter tips and arrays [3] [12].

*Xin et al. (2014)* stated that zirconium carbides have attracted much attention due to their relatively low density, low cost, excellent ablation resistance and good strength at high temperatures [9].

According to *Nam et al. (2009)*, ZrC is used in a fine powder form to produce functional textiles for thermal storage. ZrC absorbs 95 % of the solar energy impinging on the surface to produce heat. Due to these multiple properties of ZrC, it is used as a thermal storage material that effectively absorbs sunlight while allowing almost none of the collected energy to escape [12].

ZrC is being considered as a structural and fission product[1] barrier coating material for TRISO (Tri-Isotropic) coated nuclear fuel used in High Temperature Reactors (HTRs), replacing or in addition to the currently used silicon carbide (SiC) [13].

| Property (Unit) | Value | C/Zr Ratio |
|---|---|---|
| Young's modulus (GPa) | 350 – 440 | 0.77 – 0.96 |
| Poisson's ratio | 0.21 – 0.23 | 0.77 – 0.96 |
| Shear modulus (GPa) | 167 | 1.0 |
| Hardness (GPa) (Vickers) | 27 – 35 | ~1.0 |
| Fracture toughness (MPa $m^{1/2}$) | 1.40 – 2.74 | 0.93 |
| Thermal expansion (x $10^{-6}$/K) | 6.7 – 7.6 | 0.72 – 0.94 |

**Table 1: Mechanical and thermal properties of ZrC [13]**

The Young's modulus is determined for ZrC with a C/Zr ratio between 0.77 – 0.96 in the temperature range of 300 – 2300 K and measured by means of the sonic resonance technique. When the C/Zr ratio is above 0.95 the Young's modulus starts to decrease due to surplus carbon present in the sample [13]. The Poisson's ratio at 300 K increases from 0.21 to 0.23 with increasing C/Zr ratio of 0.77 – 0.96 (Table 1). Using the calculated Young's modulus and Poisson's ratio at room temperature the shear modulus for stoichiometric ZrC is 167 GPa. This data however must be rectified for porosity and no correlation between temperature and C/Zr ratio has been established [13].

The hardness of metal carbides is related to the strong hybrid ionic-covalent bonds existent in the metal structure. The ionic-covalent Zr-C bonds in ZrC are comparatively strong and thus tend to circumvent plastic deformation. The Vickers hardness of near-stoichiometric

[1] Fission products are the atomic fragments left after a large atomic nucleus fissions

ZrC is stated to be 27 – 35 GPa at 293 K, but an extensive study on the deviation of hardness with changing stoichiometry has not yet been carried out [13].

According to *Katoh et al. (2013)*, data on the fracture toughness of ZrC is limited. Thermal creep affects the failure criteria for nuclear materials such as SiC and ZrC. Stress developed due to fission product gases and other volatile fission product formation as well as $CO_2$ formed during oxidation of ZrC, can cause creep that can result in stress rupture. The thermal expansion coefficient may increase with increasing carbon vacancies and decrease when the vacancies are occupied with impurities [13].

## 2.2 Phase Chemistry and Composition of ZrC

The ZrC crystallizes in a NaCl type lattice and can display a wide range of zirconium (Zr) to carbon (C) ratios. It has been found that the pure ZrC phase exists when the molar ratio of carbon to zirconium is in the range of 0.61:1 to 1:1 at 500 $^{o}$C [17]

The ZrC phase diagram has been determined by *Guillermet (1995)* using thermodynamic calculations and previously determined phase relations. According to *Katoh et al. (2013)*, the reported diagrams must be observed at best as close approximations of the phase relations since ZrC is prone to oxygen and to some degree nitrogen contamination.

*Jackson et al. (2011)* investigated the phase relations using laser melting of prepared samples. The oxygen and nitrogen impurities were less than 1 wt % and 0.001 wt % respectively in the samples and their *(Jackson et al. 2011)* work correlated with the suggested phase relations determined by *Guillermet (1995)*.

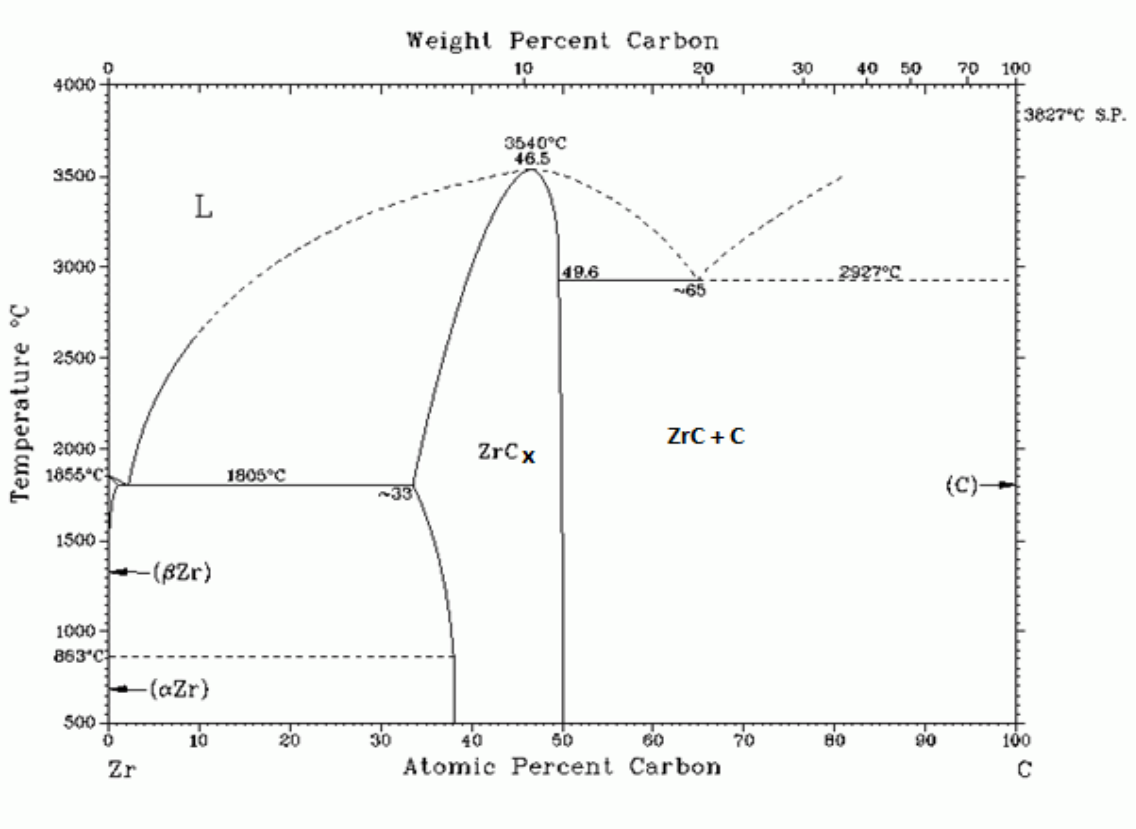


**Figure 1: The Zr-C phase diagram, [*Katoh et al. (2013), Storms (1967)*]**

Figure 1 shows the ZrC phase diagram that comprises of five condensed phases, namely:

- The β-phase: a Zr-rich solid solution with C in bcc Zr (An α-phase which formed by polymorphic transformation of the matrix of the β-phase)
- The α-phase: a Zr-rich solid solution with ZrCx in hcp Zr, which on equilibrium cooling will give rise to the exsolution of ZrCx with about 38 % atomic carbon
- The γ-phase: the sub-stoichiometric ZrCx ($0.38 \leq x \leq 0.50$, carbon in solid solution that will form laminae of ZrCx) with fcc structure
- The carbon-rich (ZrC + C) eutectic
- The liquid phase

The β phase as shown in Figure 1, are formed by the presence of small fractions of carbon in the octahedral interstitial sites of zirconium. The transformation of α to the β phase takes place between 1121 – 1159 K. The β phase melts at a temperature of between 2080 – 2133 K in the absence of carbon. The variation in temperature is due to the presence of dissolved oxygen [*Katoh et al. (2013), Storms (1967)*].

The γ phase is achieved when an appreciable amount of the octahedral interstitial sites are filled with carbon atoms *(Guillermet 1995)*. This phase's actual composition is not clear *(Katoh et al. 2013)*, but it is suggested to be between $ZrC_{0.55}$ and $ZrC_{0.98}$ *(Storms 1967)*.

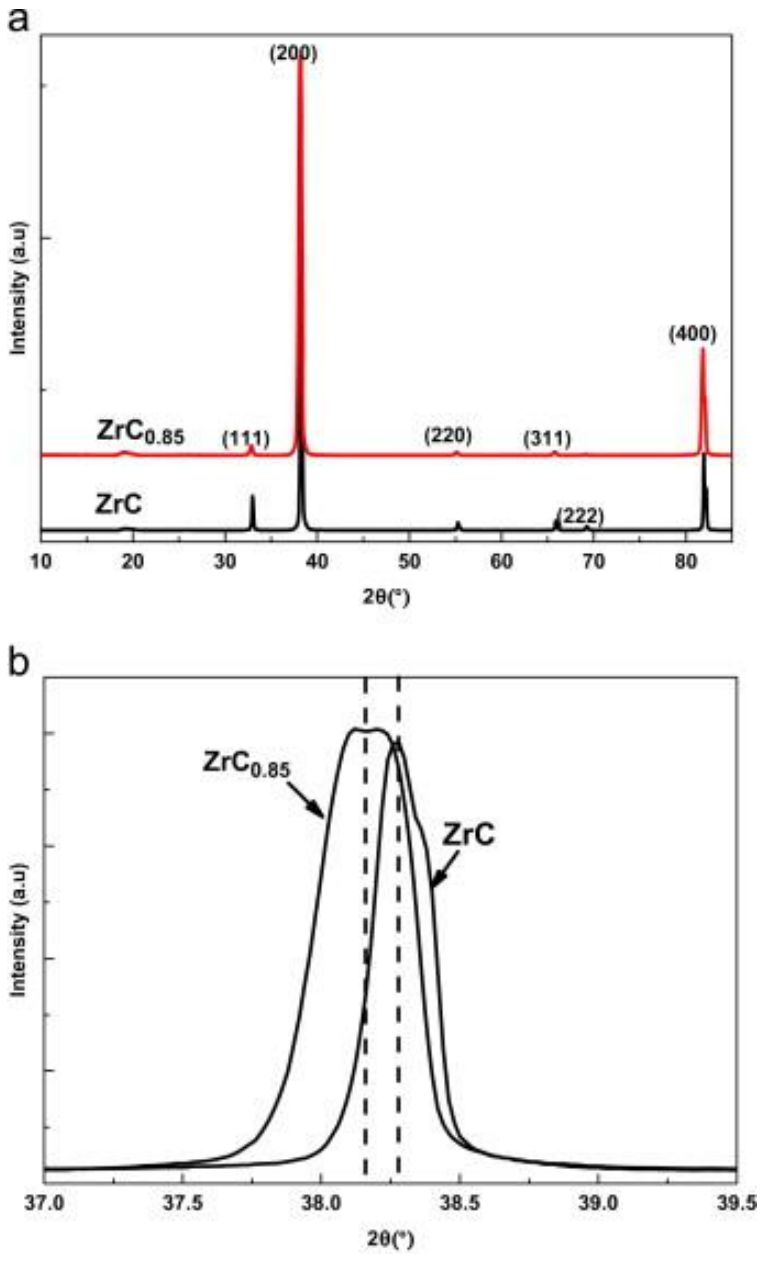


**Figure 2: XRD patterns of (a) ZrC and $ZrC_{0.85}$ coatings and (b) expanded XRD (200) peak for both spectra showing the shift in peak [17]**

Figures 2 (a & b) show the XRD patterns of ZrC coatings (ZrC and $ZrC_{0.85}$) deposited by chemical vapour deposition. The XRD spectra show that both coatings exhibit a crystalline

structure with a strong (200) texture normal to the substrate surface. Comparing the XRD spectra of both samples, it was observed that the peak position corresponding to the (200) reflection in non-stoichiometric $ZrC_{0.85}$ coating displaced slightly towards the lower 2θ value compared to the stoichiometric ZrC coating (Figure 2b). This peak shift towards a lower 2θ value in the non-stoichiometric ZrC coating was found to be in agreement with the results obtained by *Wang et al. (2011)*.

The lattice parameters of both coatings ($ZrC_{0.85}$ and ZrC) were calculated and are listed in Table 2 [17]. It was found that the lattice parameter of the stoichiometric ZrC coating was 4.692 Å, which is slightly smaller than that of the non-stoichiometric $ZrC_{0.85}$ coating (see Table 2). This is in agreement with the results reported by *Nachiappan et al. (2010)* and *Wang et al. (2011)*. They (op cit) also found a slight decrease in the lattice parameter for non-stoichiometric ZrCx with the decrease in carbon content. This can be attributed to the presence of more carbon vacancies in ZrCx (x=0–1) with the decrease in x [17].

| Sample | JCPDS | Lattice parameter (Å) |
|---|---|---|
| ZrC | 35–0784 | 4.692 |
| $ZrC_{0.85}$ | 65–8836 | 4.693 |

**Table 2: Lattice parameters calculated using XRD results of ZrC and $ZrC_{0.85}$ coatings [17]**

Figure 3 of *Long et al. (2014)*, shows the X-ray Photoelectron Spectroscopy (XPS) spectrum of ZrC coating. The peaks observed and the corresponding phases are shown on the XPS spectrum. The analysis of XPS spectra of the stoichiometric and non-stoichiometric samples confirms the presence of Zr and C atoms as surface elements. However, peaks corresponding to oxygen (O) were also observed. This meant that the surface of the coating was contaminated by oxygen to some extent and resulted in the formation a Zr–O bond [30]

and a probable ZrO phase on or intermixed with the ZrC coating applied by *Wang et al. (2011)*.

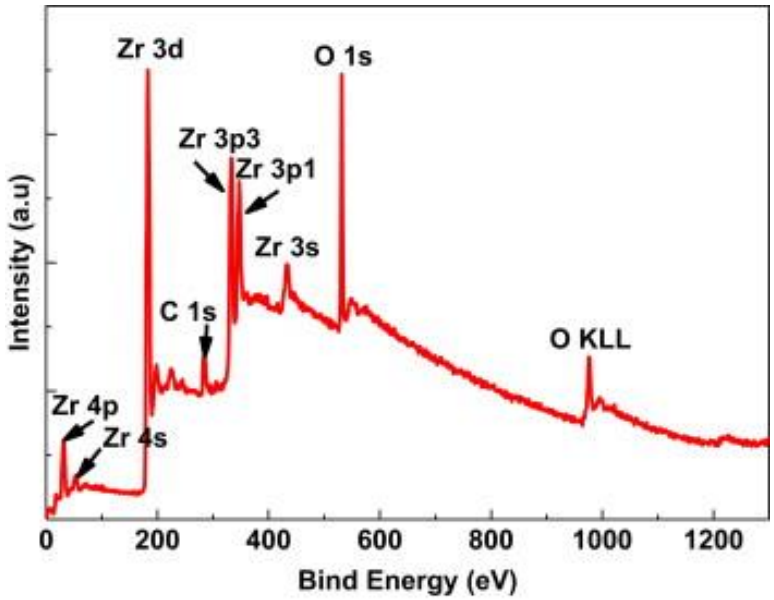


**Figure 3: XPS spectrum of ZrC coating showing the peaks appearing from different energy levels [17]**

## 2.3 Zirconium Alloys as Cladding and its Oxidation

Zirconium alloys used in nuclear reactor cores are characterized by the fact that hafnium (Hf) is removed, as Hf has a high thermal neutron capture cross section. The zirconium alloys for nuclear applications are quite limited today, they are based either on a combination of tin (1-2 %) and iron additions or on niobium addition (1-3 %) for core use. Tin was originally added at a concentration of 1.2-1.7 % to increase corrosion resistance. Zircaloys are Zr-Sn alloys. Sn also contributes to increasing the mechanical properties, mainly the creep resistance of the alloys. Iron and chromium have been added to improve mechanical properties and corrosion resistance [10]. According to *Zuev et al. (2005)*, the mechanical

properties of alloys depend largely on the alloying element concentration, as well as the state in which the alloying addition occurs in the material [14].

The Zr alloy tubes for fuel cladding and fuel assemblies have to meet the following requirements with regards to reliability and safe operation of nuclear reactors:

- Good corrosion resistance, low hydrogen pickup, and reduced oxide growth
- Dimensional stability
- High resistance to cracking and
- Safe operation under critical and changing operating conditions.

The investigation of *Abolhassani et al. (2005)* identified that, irradiation-induced structural changes and alteration of elemental and phase composition cause variation in the mechanical properties of the Zr alloy cladding material through continued exposure. The irradiation effects on the oxidation rate of zirconium alloys have been observed by several studies [15] and the shared agreement is that the material can have a different behaviour after a long-term stay in the reactor. Observations on one material under specific reactor conditions do not always extrapolate to other conditions. This conclusion would suggest that the mechanism of oxidation in the reactor deviates at a certain stage from that of oxidation in an autoclave. Additionally, it implies that, more than one mechanism is involved in the oxidation of the material in a reactor, especially at different stages of oxidation [15].

The study of *Abolhassani et al. (2005)* showed that, oxidation of zirconium alloys at high temperatures is governed by the diffusion of the oxidizing species to the metal-oxide

interface. The stresses in the oxide due to the Pilling-Bedworth parameter[2] are compressive and as an example Zircaloy-4 (metallic phase) at the interface, is reported to be under a tensile stress and the oxide under a compressive stress. In the case of precipitate containing alloys, metallic precipitates do not oxidize before they are totally surrounded by the oxide. Irradiation is considered as one of the causes of faster oxidation for the dissolution of alloy oxide precipitates [15].

Zirconium has a very high affinity for oxygen which creates difficulty for industrial processing of Zr and Zr alloys. Thus, in contact with water or air, it is immediately covered with a protective oxide layer, which gives an excellent resistance to corrosion [10].

According to *Yueh et al. (2005)*, the waterside corrosion of fuel cladding in Light Water Reactors (LWR) is generally recognized as one of the main limiting factors in achieving high fuel burnups[3]. ZIRLO[4] was introduced for use in Pressurized Water Reactors (PWRs) as demonstration rods in 1987. Since then, over three million ZIRLO clad fuel rods have been used in more than fifty PWRs in support of increasing fuel burnups. Parallel to the increase in fuel utilization was an increase in fuel duty that further challenged the corrosion performance of advanced zirconium alloys. In addition to the corrosion performance improvements achieved by ZIRLO cladding relative to Zircaloy-4, ZIRLO exhibited lower in-reactor creep, resulting in better dimensional stability [16].

[2] Pilling-Bedworth parameters are the atomic or molecular mass, number of atoms of metal per one molecule of the oxide, density and the molar volume
[3] Fuel burn up is a measure of how much energy is extracted from a primary nuclear fuel source
[4] ZIRLO is a Zr alloy with 1 % niobium, 1 % tin and 0.1 % iron

The experiments conducted by *Yueh et al. (2005)* showed that, during the development of ZIRLO, lower uniform corrosion in autoclave tests (in pure water and steam) and in reactors were achievable for binary Zr-Nb alloys. The primary difference between ZIRLO and Zr-Nb binary alloys is the presence of tin in ZIRLO. While the presence of tin increases the uniform corrosion of the alloy, it also improves the creep strength of the material and eliminates the accelerated corrosion observed when testing in 633K water containing 70 ppm lithium and localized or nodular corrosion witnessed in reactor, thereby providing a more robust alloy [16].

*Yueh et al. (2005)* stated that efforts to improve the performance of the ZIRLO alloy started when variations from the nominal Zr-1%Nb-1%Sn-0.1%Fe composition and variations in thermal processing were explored. This approach was similar to the studies undertaken in the industry during the 1980s to improve the performance of Zircaloy-4 in which a reduction of tin and increasing second phase particle (SPP) size were identified [16]. The goal of the above-mentioned study was to lower the uniform corrosion of ZIRLO, to maintain corrosion resistance in lithiated water, to maintain a preferred microstructure and to achieve acceptable mechanical properties such as strength and thermal creep [16].

## 2.4 Deposition of ZrC

According to *Velasco et al. (2014)*, surface engineering is rapidly evolving to an extent that surface modification of widely used materials allows engineers to convert a material with poor mechanical or corrosion resistance into a useful product in which only few microns or even nanometres of the surface have been modified for such purpose [7].

*Vasudevamurthy et al. (2008)* stated that, coatings play a vital role ranging from under-sea to space applications including communications, sensors, satellites, optics, auto and aerospace industries. High temperature components of gas-turbine engines for aircraft, such as, air foils and vanes are coated with metallic and ceramic coatings to improve performance and reliability. Hence, there is a constant effort to engineer surface properties of materials increasing the life of components under severe environmental conditions where factors like corrosion, high temperature oxidation and wear are concerns. Likewise, multi-layered ceramic and metallic films are widely used in the manufacture of microelectronic and communication components [5].

It is important to understand the inter-relationship of applications, coatings and processes. Applications dictate the selection of coating materials and the desired thermal, chemical and mechanical properties, often determine the deposition method and processing parameters *(Vasudevamurthy et al. 2008)*.

Coating processes can be largely classified into two groups, that is, metallic and non-metallic as shown in Figure 4. Metallic coatings can be grouped into vapour deposition, hard facing and miscellaneous techniques. Vapour deposition includes Physical Vapour Deposition (PVD) and Chemical Vapour Deposition (CVD). Hard facing is divided into welding, thermal spraying and cladding. Each of these processes, as shown in Figure 4 has its advantages and disadvantages. The chemical and physical conditions during the deposition reaction can strongly affect the composition, residual stresses and microstructure of the coating. According to *Vasudevamurthy et al. (2008)*, the desired coating thickness and material

properties[5] are dictated by its application, which will determine the coating deposition process to be used [5]. The applications in microelectronics or nuclear technology require rather thin and high quality films *(Abolhassani et al. 2005)*.

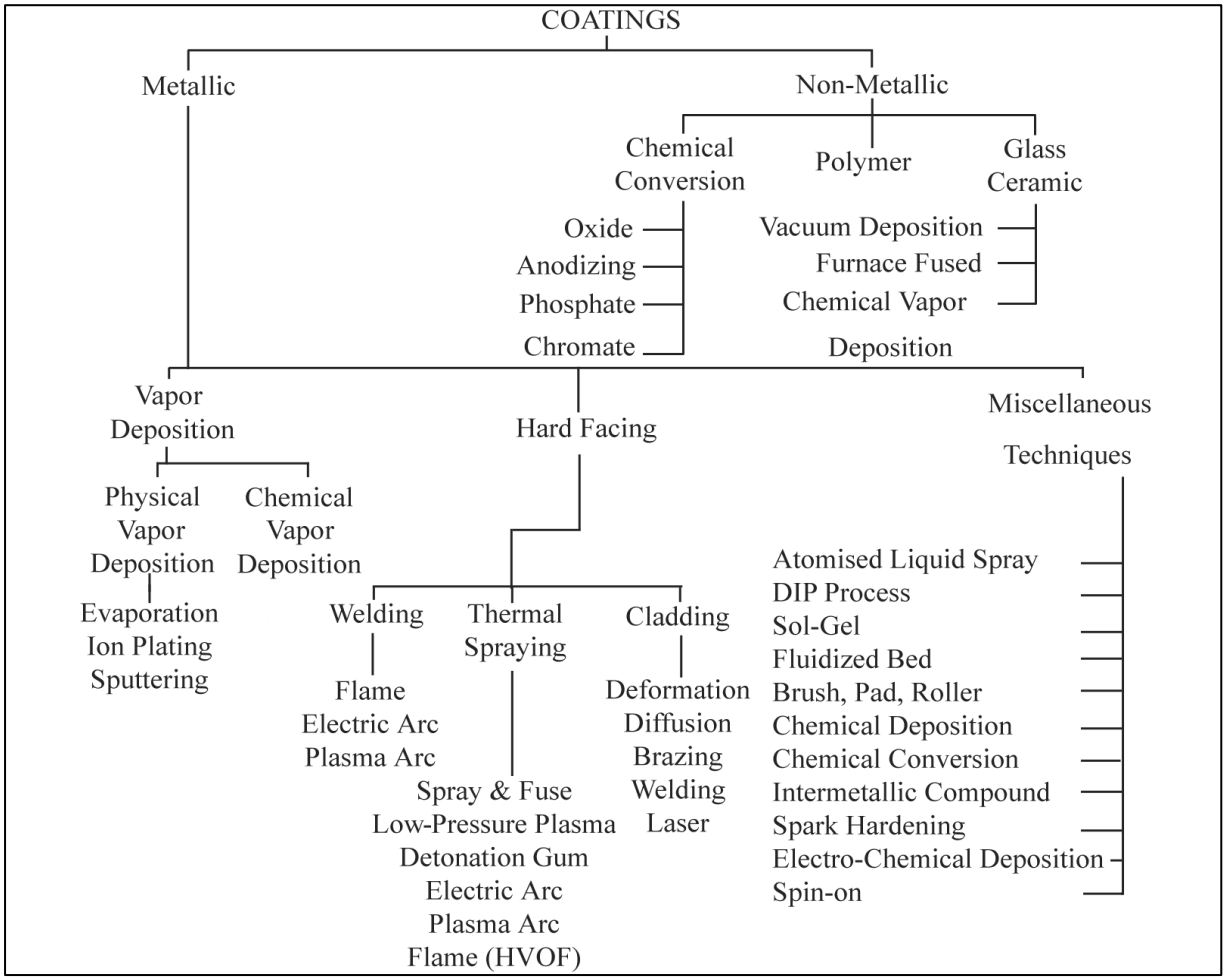


**Figure 4: Different coating deposition techniques that are currently used within the coating industry [8]**

ZrC thin films have been deposited using various techniques, such as:

- Chemical vapour deposition (CVD)
- Pulsed laser deposition (PLD)

[5] Including microstructure, physical and mechanical properties

- Reactive melt infiltration (RMI)
- Physical vapour deposition (PVD)
- Plasma spraying (PS)

The details on these techniques are discussed in Sections 2.4.1 to 2.4.5.

### 2.4.1 Chemical Vapour Deposition

The Chemical Vapour Deposition (CVD) is a widely used materials processing technology with the majority of its applications involving the application of solid thin film coatings to surfaces. CVD involves blowing a precursor gas or gases into a chamber containing one or more heated objects to be coated. Chemical reactions occur on and near the hot surfaces, resulting in the deposition of a thin film of specific composition. The deposit can also be obtained by reaction between the precursor gases in the vapour phase or by a reaction between a constituent of the vapour phase and the surface of the substrate. These processes may be accompanied by the production of chemical by-products that are exhausted out of the chamber along with unreacted precursor gases.

The CVD process depicted in Figure 5 is extensively used to deposit ceramic coatings. The use of zirconium tetrachloride ($ZrCl_4$) as a source material for zirconium provides an easy control on the flow of $ZrCl_4$ vapours when it enters into the CVD furnace during the CVD process. Using the CVD process, many research groups have successfully manufactured near theoretical density and oxide-free condensates of hard ceramic coatings *(Long et al. 2014)*.

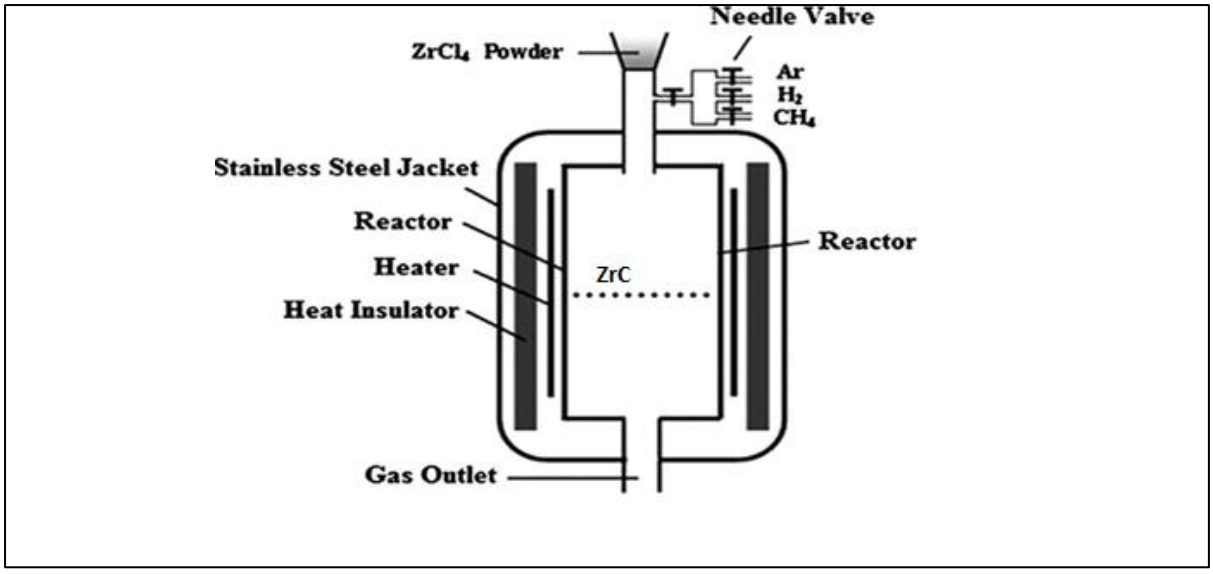


**Figure 5: A schematic diagram of a Chemical Vapour Deposition (CVD) setup of zirconium carbide (Long et al. (2014)**

According to *Long et al. (2014)*, it has been observed that the phase composition, microstructure and mechanical properties of hard ceramic coatings, such as, SiC and ZrC produced by CVD, are greatly affected by the chosen combination of deposition parameters such as gas-flow rate, molar ratio of different species, deposition temperature and substrate position [17].

*Long et al. (2014)* produced two sets of ZrC coatings by CVD with different Zr to C ratios[6]. Their phase composition, microstructure, surface chemistry and mechanical properties were studied using standard techniques, such as, X-ray Diffraction (XRD) and scanning electron microscopy (SEM). Surface chemistry of both coatings was analysed by applying a surface sensitive technique, such as, X-ray Photoelectron Spectroscopy (XPS).

Zirconium carbide (ZrC) coating production by CVD is as follows. The ZrC were produced on graphite substrates by CVD at a temperature of 1550 ± 5 $^{o}$C. High purity graphite substrates

[6] That is, stoichiometric ZrC and non-stoichiometric $ZrC_{0.85}$

of the size (30 x 20 x 5) $cm^3$ were placed in a hot zone of the CVD reactor and the coating was allowed to grow for 3 hours. The substrates were cleaned ultrasonically in acetone solution, followed by cleaning with ethanol before deposition. After substrate cleaning, substrates are placed on the substrate table. For the ZrC coating, zirconium tetrachloride ($ZrCl_4$) powder of 99.9 % purity was used as a source material for Zr and high purity methane ($CH_4$) was used for C. The purified hydrogen ($H_2$) gas was used as a reducing agent for $ZrCl_4$, and argon (Ar) gas was used as carrier and dilution gas. In the CVD reactor, ZrC coatings are formed as a result of the following chemical reactions *(Long et al. (2014)*:

$$\mathbf{ZrCl_4 + H_2 \rightarrow ZrCl_x + HCl\ (}\boldsymbol{x}\mathbf{ = 0, 1, 2, 3)} \qquad \mathbf{(1)}$$

$$\mathbf{CH_4 \rightarrow C + 2H_2} \qquad \mathbf{(2)}$$

$$\mathbf{ZrCl_x + C \rightarrow ZrC + }\boldsymbol{x}\mathbf{Cl} \qquad \mathbf{(3)}$$

$$\mathbf{2Cl + H_2 \rightarrow 2HCl}\ [17] \qquad \mathbf{(4)}$$

Many research studies have been carried out to investigate the effect of different parameters on the CVD process and the ZrC product [17]. However, understanding the deposition mechanism of ZrC from $ZrCl_4$ is essential to control the deposition process. In the study of *Wang et al. (2011)*, thermodynamic calculations were carried out and the deposition rates at different temperatures were investigated. The results obtained from this study show that carbon and zirconium deposit separately and that the deposition process is controlled by the carbon deposition rate [31].

According to *Craciun et al. (2013)*, when the hydrogen concentration used in this work was reduced, the decomposition of $ZrCl_4$ was stopped and less ZrC obtained, however, the

carbon deposition was promoted with less hydrogen. This is because the carbon deposits faster with increasing reaction temperature when compared to zirconium [3].

### 2.4.2 Electron Beam Physical Vapour Deposition

Electron Beam Physical Vapour Deposition (EB-PVD) is a form of physical vapour deposition in which a target anode is bombarded with an electron beam given off by a charged tungsten filament under high vacuum. The electron beam causes atoms from the target to transform into the gaseous phase. These atoms then precipitate into solid form, coating everything in the vacuum chamber.

*Singh et al. (2005)* described how EB-PVD can be used as a simple process in which a focused high energy electron beam is directed to melt evaporant material(s) in a vacuum chamber. The evaporating material condenses on the surface of the substrate or components resulting in the formation of a deposit referred to as a coating. During deposition, external heating is frequently applied to the substrate for increasing metallurgical bonding between the coating and the substrate. Using the EB-PVD process, uniform coating of complex parts, such as, turbine air-foils can be accomplished by continuous rotation in a vapour cloud [18].

Figure 6, shows the schematic of an EB-PVD system in an electromagnetic alignment configuration.

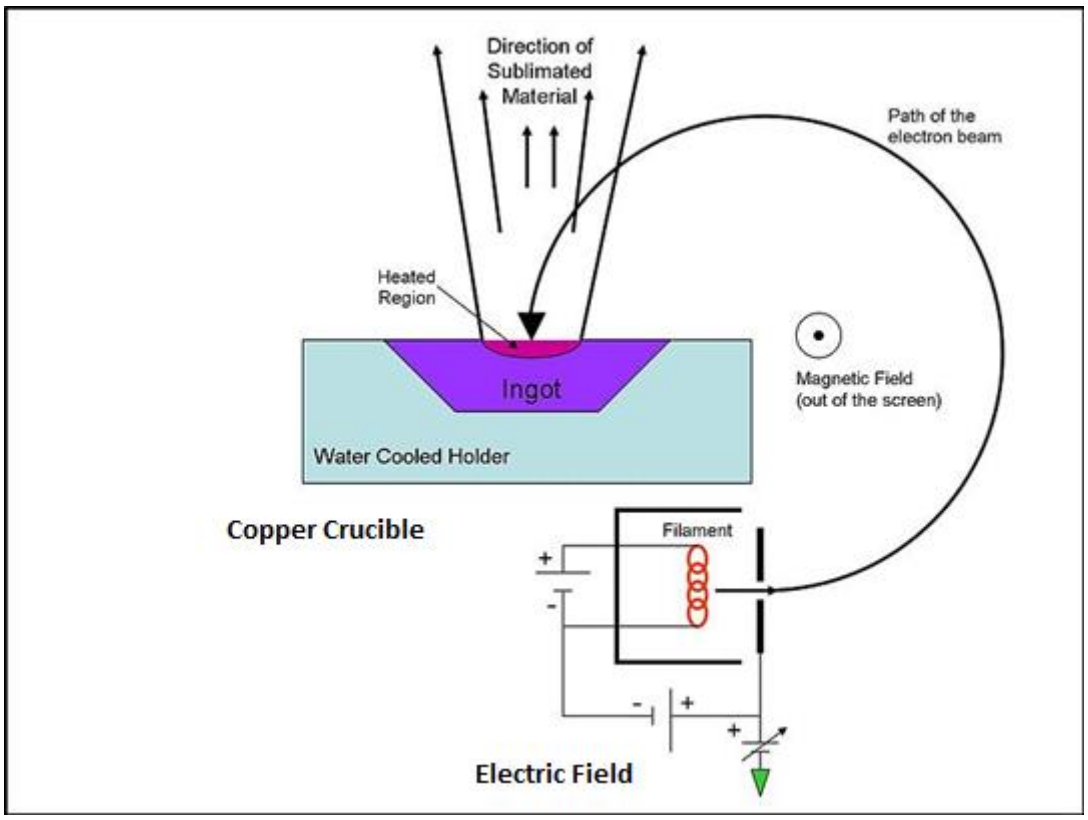


**Figure 6: The schematic of an EB-PVD (Electromagnetic Alignment) system**

In Figure 6, the ingot is held at a positive potential relative to the filament. In order to avoid chemical interactions between the filament and the ingot material, the filament is kept out of line of sight. A magnetic field is employed to direct the electron beam from its source to the ingot position. An additional electric field can be used to navigate the beam over the ingot surface allowing uniform heating.

The three main EB-PVD configurations are electromagnetic alignment, electromagnetic focusing and the pendant drop configuration. Electromagnetic alignment and electromagnetic focusing use evaporation material that is in the form of an ingot while the pendant drop configuration uses a rod. Ingots will be enclosed in a copper crucible while a rod will be mounted at one end in a socket. Both the crucible and socket must be cooled.

This is typically done by water circulation. In the case of ingots, molten liquid can form on its surface which can be kept constant by vertical displacement of the ingot.

The EB-PVD unit consists of 4 main components, namely,

- an electron beam (EB) gun assembly
- a water cooled copper crucible which contains the material to be evaporated
- the substrate, and
- a vacuum chamber unit for a variety of coating applications.

The evaporant material is placed in a water-cooled copper crucible, which could be either pocket type for small volume evaporation applications or continuous ingot feeding through a copper-cooled crucible for large volume evaporations *(Singh et al. 2005)*.

According to *Singh et al. (2005)*, the EB-PVD process provides many appropriate processing characteristics, such as, relatively high deposition rates, dense coatings, controlled composition, tailored microstructure, low contamination and flexible deposition parameters. EB-PVD process produced coatings, usually have a good surface finish and a uniform microstructure. By manipulating the process parameters and ingot compositions, the microstructure and composition of the coating can be easily changed. Thus, multi-layered ceramic and metallic coatings can be readily formed and various metallic and ceramic coatings (oxides, carbides and nitrides) can be deposited at relatively low temperatures. Even elements with low vapour pressure, such as, molybdenum, tungsten, rhenium and carbon are readily evaporated by this process [18]. Zirconia and hafnia based thermal barrier coating materials were produced by industrial prototype electron beam-physical vapour deposition (EB-PVD) [33].

### 2.4.3 Pulsed Laser Deposition (PLD)

The Pulsed Laser Deposition (PLD) technique uses a high power laser to melt, evaporate and ionize a target material, known as ablation. The ablation will then produce luminous plasma which will expand away from the target material towards the substrate where condensation and the formation of the thin layer takes place.

*Zuev et al. (2005)* stated that Pulsed Laser Deposition (PLD) is one of the most versatile research techniques which permit for relatively low to moderate deposition temperatures of refractory carbides and nitrides without compromising their crystalline quality [14]. PLD allows for a decrease of the substrate temperature with respect to other techniques while preserving the high quality of the deposited films and this has been successfully used to deposit thin ZrC films [18]. An experimental setup for a typical PLD system is shown in Figure 7.

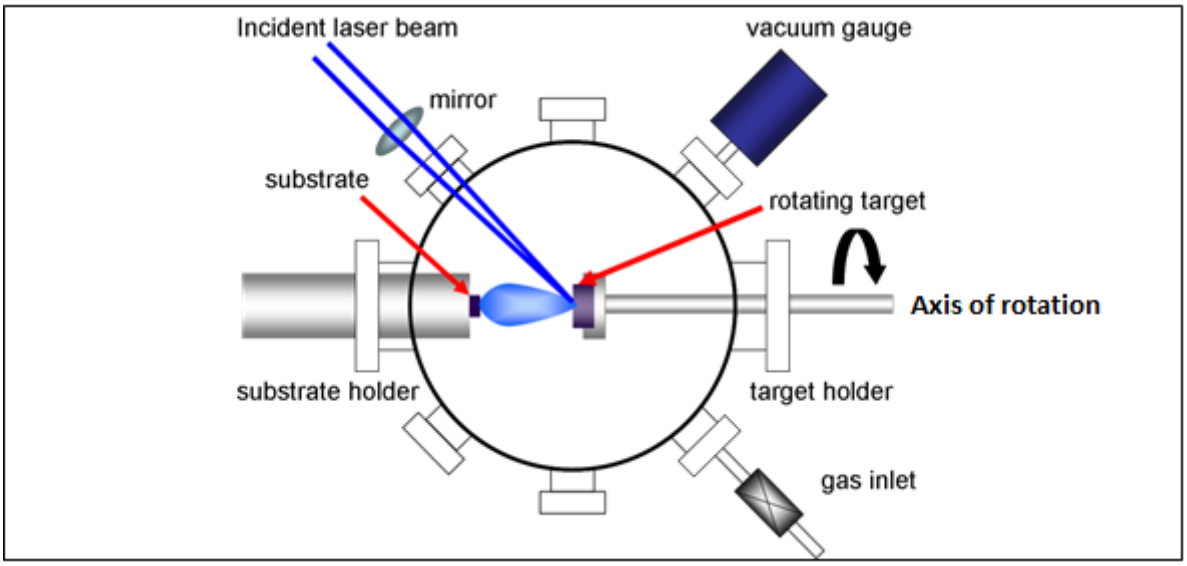


**Figure 7: Schematic diagram of a Pulsed Laser Deposition system setup [19]**

It consists of two major components, that is, the external laser source and the stainless steel vacuum chamber. The vacuum chamber can be placed directly facing the output laser pulse or be set at certain angles. For the latter case, a reflecting mirror is necessary. Inside the PLD chamber, a target and a substrate holder are aligned on the same line but are separated by a distance of 3 cm to 5 cm. Such a distance range has been experimentally confirmed for proficient laser ablation. When the incident focusing laser beam bombards the rotating target, the rise of the localized temperature causes vaporization of the material. It is a characteristic of plasma plume with high energetic species[7]. The film growths depend on several parameters, such as, laser fluence, laser repetition rate, substrate temperature and vacuum level. By adjusting the number of laser pulses on the targets, different layers with controllable thicknesses can be produced.

Some of the mechanical properties of ZrC reported by *Zuev et al. (2005)*, were measured on films deposited using the PLD technique. In addition, it has been showed that by using a higher repetition rate laser for ablation, the substrate temperature could be reduced to only 300 $^{o}$C while the film growth rate is increased and the crystalline quality maintained [14].

*Craciun et al. (2009)* presented the results of an investigation using the PLD method to deposit ZrC at different deposition conditions. They used a KrF excimer laser to ablate a ZrC target within a stainless steel chamber under a $CH_4$ gas environment. The substrate used was Si at an optimum substrate temperature of 300 $^{o}$C. Deposited dense layers ranged from 17-22 Å [23].

[7] For example, ions, electrons, atoms, molecules, clusters, particulates and molten globules

*Craciun et al. (2009)* found that the main obstacles in obtaining high quality ZrC films include the high melting point of ZrC, low sputtering or evaporation rates and the affinity of Zr for oxygen [6].

In order to obtain high crystalline quality, rather extreme deposition conditions has to be used, such as, substrate temperatures in excess of 700 $^{o}$C, with a vacuum better than $2\times10^{-6}$ Pa and a laser fluence of around 10 J/cm$^2$. These conditions can be very challenging for easy implementation on a large industrial scale application [6].

According to *Craciun et al. (2009)*, Si substrates were cleaned in acetone and ethanol, then rinsed in deionized water, and finally blown dry with high purity nitrogen before being loaded into the deposition chamber. The nominal substrate temperature was set at 300 $^{o}$C. Depositions were performed under a high purity atmosphere of $CH_4$ or Ar ($2\times10^{-3}$ to $10^{-2}$ Pa). After the deposition, the films were slowly cooled to room temperature (under the same atmosphere as that used for deposition), but at a much higher pressure of around 104 Pa *(Zuev et al. 2005)*.

*Craciun et al. (2009)* reported that the PLD technique, allowed for an easy control of crystalline structure, composition and defects concentration control in deposited thin films. By using PLD, very hard TiN films were deposited by *Craciun et al. (2009)* at a moderate substrate temperature of only 300 $^{o}$C. Despite the widespread use and research, the process of material transfer from the target to the substrate is not yet fully understood.

### 2.4.4 Reactive Melt Infiltration (RMI)

Reactive Melt Infiltration (RMI) is another coating technique conducted at high temperature. *Xin et al. (2014)* reported the preparation of ZrC coating with a dense structure by RMI at high temperature. When comparing this technique to the CVD process, RMI is more suitable for preparing ceramic coatings for its certain advantages, such as, low cost, easy operation and no special requirements to the complex gas feed stream system. The bonding ability of the coating with the substrate can be enhanced by the reactions occurring between the substrate and coating materials [9].

According to *Xin et al. (2014)*, a graphite substrate with a density of 1.76 g/cm$^3$ was used for coating by RMI and then cut into small specimens of (10 × 10 × 10) mm$^3$. The specimens were hand-polished using 600 grit SiC paper before the coating process and cleaned ultrasonically with ethanol and dried at 120 $^{o}$C for 2 h. Zirconium powder of 48 μm was placed around the graphite samples in a graphite crucible. Then, the samples were heated up to 2000 $^{o}$C under a pressure of 200 Pa. At temperatures higher than the zirconium melting point, the zirconium powder melted and reacted with the graphitic carbon to form the ZrC coating. The whole coating process was conducted at temperatures within the range of 2000−2300 $^{o}$C for 1 h, followed by a natural cooling course [9].

### 2.4.5 Plasma Spraying

The Plasma Spray Process comprises spraying molten or heat-softened material onto a substrate surface to provide a coating. Material in powder form is injected into a very high temperature plasma flame, where it is rapidly heated and accelerated to a high velocity. The hot material impacts on the substrate surface and rapidly cools to form the coating. This

process is sometimes referred to as a cold process, since the substrate temperature can be kept low during processing thus avoiding damage, metallurgical changes and distortion to the substrate material.

The plasma spray process is most commonly used in normal atmospheric conditions and referred to as Atmospheric Plasma Spray (APS). Some plasma spraying is conducted in protective environments using vacuum chambers normally back filled with a protective gas at low pressure. This is referred to as Vacuum Plasma Spray (VPS) or Low Pressure Plasma Spray (LPPS).

According to *Zhu et al. (2011)*, the Plasma Spraying (PS) technique is facilitated under different plasma conditions. The conventional plasma-spray technique has been widely used to deposit metal, ceramic or composite coating materials in order to meet the different application requirements, such as power source, automobile, aerospace, electronics, nuclear engineering and biomedicine [4]. Plasmas can be produced by a number of discharge types together with direct-current (DC) discharges, low-frequency discharges (kHz range), Radio-Frequency (RF) discharges (MHz range) and microwave discharges (GHz range) [34].

According to *Matejka & Benko (1989)*, PS is the most versatile thermal spray process available today because of its ability to spray a large variety of materials.

According to *Katoh et al. (2013)*, it is difficult to obtain dense, super-thin and defect-free coatings with this procedure. In contrast, vapour phase deposition processes (PVD or CVD) can deposit such a high-quality coating product, whereas high operating cost and low deposition rate strongly restrict vapour phase deposition processes' application ranges [13].

According to *Matejka & Benko (1989)*, PS devices use an arc which is formed between two electrodes inside a gas which forms the plasma. This gas usually consists of either an argon/hydrogen or argon/helium mixture. As the plasma gas is heated by the arc, it expands and is accelerated through a shaped nozzle, creating velocities up to MACH 2 and temperatures within the arc zone easily approaching 10 000 $^{o}$C. In this process, the coating material is injected into the hot plasma in the form of a powderous feedstock, melted and accelerated. When these particles impact the substrate, the material solidifies and builds up into a typical lamellar structure. These coatings usually do not need any post-treatment after spraying [20]. Although most plasma spraying is done in a vacuum chamber the process can also be done at atmospheric conditions. PS has a fast deposition rate, resulting in a relatively dense layer having good adhesion. Figure 8 shows the schematic diagram of the plasma spray process.

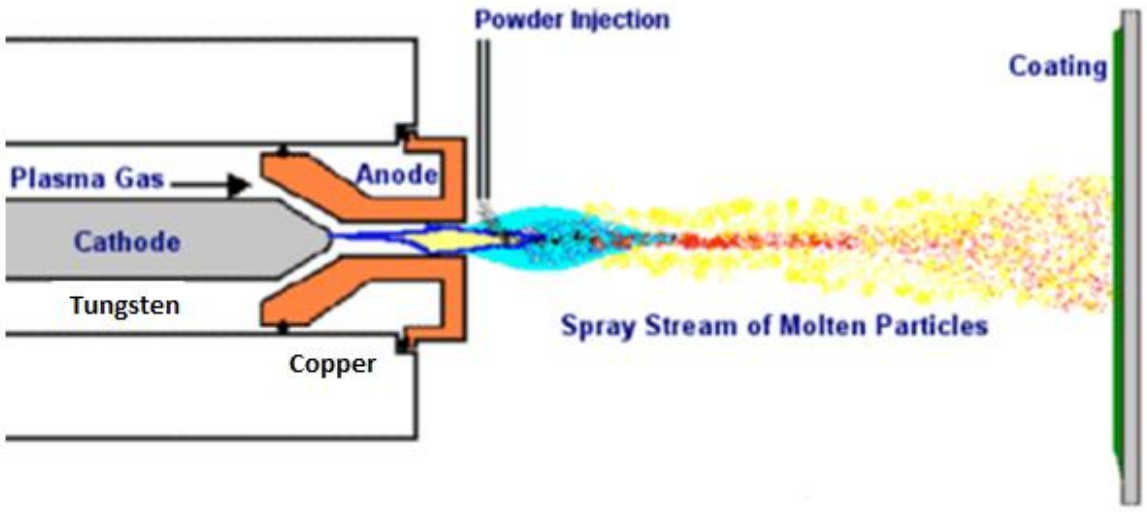


**Figure 8: Schematic diagram of a typical plasma spray process**

In Figure 8, the plasma gun is comprised of a copper anode and tungsten cathode, both of which are water-cooled. The plasma gas, typically argon, nitrogen, hydrogen or helium, flows around the cathode and through the anode, which is a constricted nozzle. The plasma is initiated by a high voltage discharge that causes localized ionization and a conductive path for a DC arc to form between the cathode and anode. The resistance heating from the arc causes the gas to reach extreme temperatures, dissociate and ionize to form plasma. The plasma exits the anode nozzle as a free or neutral plasma flame or plasma which does not carry electric current.

To produce high-quality coatings with a homogeneous structure and efficient adhesion, it is important to ensure the uniform distribution of the powder particles in the plasma jet and complete melting of the particles prior to collision with the surface of the component. Therefore, one of the methods of improving the quality of plasma coatings is the reduction of the initial particle size of the powder materials. Another method of improving the characteristics of the plasma coatings which has been the subject of special attention in recent years is the formation of coatings with a nanocrystalline structure *(Frolova et al. 2011)*.

With the development of nanoscience and nanotechnology, the interest in the preparation of nanostructured coatings is growing, since they have greatly improved mechanical properties in engineering. Recently, plasma sprayed ceramic coatings using nano-sized powders have become attractive. According to *Bai et al. (2012)* plasma sprayed coatings using nano-sized powders showed high thermal shock resistance.

#### 2.4.5.1 Atmospheric plasma spraying (APS) system

In the atmospheric plasma spray (APS) process, the plasma source is supplied by a DC (Direct Current) arc plasma torch. The plasma jet is generated by a continuous electric arc between two electrodes as either a plasma gas in its pure form or a binary mixture or a ternary mixture of monoatomic gas. Powder particles are injected into the plasma jet and are then melted, accelerated and collided into a substrate previously prepared. At impact onto the substrate, the molten or semi-molten particles flatten, solidify and form the coating resulting from their layering.

According to *Lu et al. (2014)*, atmospheric plasma-sprayed coatings often display a lot of defects, including pore, crack, void, delamination, unmelted powder particles, contamination and oxidation, which are mainly caused by relatively low-velocity melted particles impacting on the substrate and weakened coating performance [11].

The ablation resistant property of ZrC-W composite coatings was studied by using the atmospheric plasma spray equipment. The flame temperature used was about 2000 $^{o}$C [9].

*Lu et al. (2014)* reported that the XRD patterns of the ZrC-W composite coatings demonstrated that the coatings were composed of cubic ZrC, cubic W and a small amount of tetragonal $ZrO_2$. The surface roughness of the composite coatings decreased with the increase of W content, which was supposed to be the result from the well melted and flattened W particles [11].

The ZrC-W composite coatings with different contents of W were effectively achieved by using the atmospheric plasma spraying technology. The ZrC-W composite coatings presented dense and lamellar microstructure, having lower surface roughness and porosity

relative to the pure ZrC coating. The ZrC-W composite coatings displayed excellent ablation and thermal shock resistant properties at high temperature, indicating that the addition of W is good for improving the ablation and thermal shock properties of ZrC coating *(Lu et al. 2014)*.

#### 2.4.5.2 Plasma Spray-Physical Vapour Deposition

According to *Mauer et al. (2013)*, Plasma Spray-Physical Vapour Deposition (PS-PVD) is a new spray process that was developed as an extension of the low pressure plasma spray process (LPPS), also known as vacuum plasma spraying (VPS). Due to the low chamber pressure in LPPS, the deposition profile is broadened and more homogeneous so that the coating area becomes enlarged and relatively thin. Dense ceramic coatings can be obtained for special applications such as solid oxide fuel cells, gas separation membranes and wear protection. By increasing the plasma power, the feedstock powder can be evaporated so that a deposit can be formed from the gas phase instead of liquid phase [22].

PS-PVD is anticipated to combine the advantages of thermal spraying (of high deposition rates and cost-efficiency) with the special feature of PVD-type processes to deposit columnar structured coatings or dense, gas-tight coatings as well [22].

#### 2.4.5.3 Low Pressure Plasma Spraying (LPPS)

The plasma spray process is most commonly used in normal atmospheric conditions and referred to as APS. Some plasma spraying is conducted in protective environments using vacuum chambers normally back-filled with a protective gas at low pressure, this is referred to as LPPS. The LPPS process usually uses a high-power plasma torch, such as, O3CP type

made by Sulzer Metco that deliveres up to 180 kW, for producing a large amount of vapour phase to form PVD-like coatings [4].

According to *Lu et al. (2014)*, the Low Pressure Plasma Spray-Thin Film (LPPS-TF) process uses low pressure conditions. In the past decade, LPPS-TF have been well studied and developed as a new generation of thermal spray process, because it significantly combines the advantages of both conventional plasma spray and vapour processes. This process allows depositing super thin and dense coatings onto large-scale or complex component surfaces in a short coating time under a relatively low operating pressure (<10 mbar), which has opened a brand-new gate for wide ranging market areas [11].

According to *Zhu et al. (2011)*, during the LPPS process, the preheated substrate can increase the contact temperature and reduce the viscosity of the impinging melted droplets and the thermal stress, and the low pressure ambience can considerably improve particle velocities and kinetic impact energies, leading to coating structure densification [4].

#### 2.4.5.4 Plasma Assisted Chemical Vapour Deposition

In the plasma assisted chemical vapour deposition method the substrate is exposed to one or more volatile precursors, in the presence of the cold plasma, which react or decompose on the surface to produce a deposit. The plasma enhances the rate of reaction on the substrate surface.

In thermal CVD, the gas-phase reactive species are produced by heating of initial reactants. In plasma CVD, the plasma energy supplied by an external RF source takes the place of heating to produce the species that afterward react and deposit on the substrate surfaces. Significantly, excessive heating and degradation on the substrate can be avoided by using

plasma electron kinetic energy instead of thermal energy. When compared to conventional CVD processing, ion bombardment can be used to modify film characteristics at much lower processing temperatures generating reactive species [35].

According to *van der Walt et al. (2015)*, plasma processing has numerous potential applications in nuclear science and technology and for the manufacturing of nuclear related materials. Over a period of three decades, the Nuclear Energy Corporation of South Africa (NECSA) has developed plasma applications in the nuclear fuel cycle, as well as the manufacture of nuclear ceramics used in nuclear reactors [32].

In recent years, new materials requirements and lower-processing-temperature requirements in solar energy cells, flat-panel displays and optical systems have made plasma assisted deposition processes increasingly important. One of the major advantages of plasma deposition processing is its flexibility for depositing films with desirable properties. In plasma-assisted CVD, this can be accomplished by varying deposition parameters such as temperature, RF power, pressure, reactant gas mixture ratio and type of reactant [35].

## 2.5 Summary

Currently, ZrC coatings are usually deposited on carbon materials by chemical vapour deposition (CVD). However, due to the low deposition rate, the coating process is time consuming, thus increasing the manufacturing cost and their applications are limited. To be able to expand their applications in ultrahigh temperature environments, new methods that can prepare dense ZrC coatings are critical and vital [9].

After all the coating processes have been reviewed, it can be recommended that plasma assisted chemical vapour deposition is the process suited for the application of coating Zr alloy fuel rods with ZrC for nuclear applications. The selected modified method should produce a dense uniform coating with excellent adhesion, be reproducible and of reasonable cost. Although the above method has successfully been used to deposit layers, such as, silicon carbide onto different substrates, the application of ZrC onto metal surfaces, such as, zirconium alloys is still in its infancy and not well understood.

Hence, the technique plasma assisted chemical vapour deposition was adopted for this project. The technique used was the inductively coupled radio-frequency plasma assisted chemical vapour deposition operated at low-pressure, thus it is also known as the cold plasma method. The experimental set up is described in Chapter 3.

# Chapter 3

# Experimental Setup and Procedure

## 3.1 Experimental Setup and Materials used

This chapter discusses the experimental apparatus setup, stoichiometry, materials used, calibration of the reactor temperature and experimental procedures used to conduct the plasma assisted chemical vapour deposition experimental work. The descriptions of the experimental apparatus setup are presented first, followed by the experimental procedures. Figure 9 represents the schematic diagram of the whole experimental setup which consists of a quartz reactor tube, generator and its controls, induction coils, gas cylinders of hydrogen and methane and its piping connections (fittings, flow meters and valves) with flow controls such as single-stage regulators, position of $ZrCl_4$ powder in a stainless steel crucible (boiling point of $ZrCl_4$ is 331 $^oC$ and the melting point of $ZrCl_4$ is 437 $^oC$) and mild steel substrate and the vacuum pump. This experimental setup was used to investigate whether it is possible to accomplish deposition of ZrC on a mild steel substrate at low pressure using $ZrCl_4$ (anhydrous, powder, 99.99 % trace metals basis, <50 ppm hafnium), $H_2$ (99.999 % purity) and $CH_4$ (total impurities less than 10 ppm, $N_2$- <5 ppm, $O_2$- <2 ppm, Ethane – <5 ppm, Moisture- <1 ppm). Mild steel was selected and used as substrate for all the experiments instead of zirconium alloy as it is much cheaper and readily available.

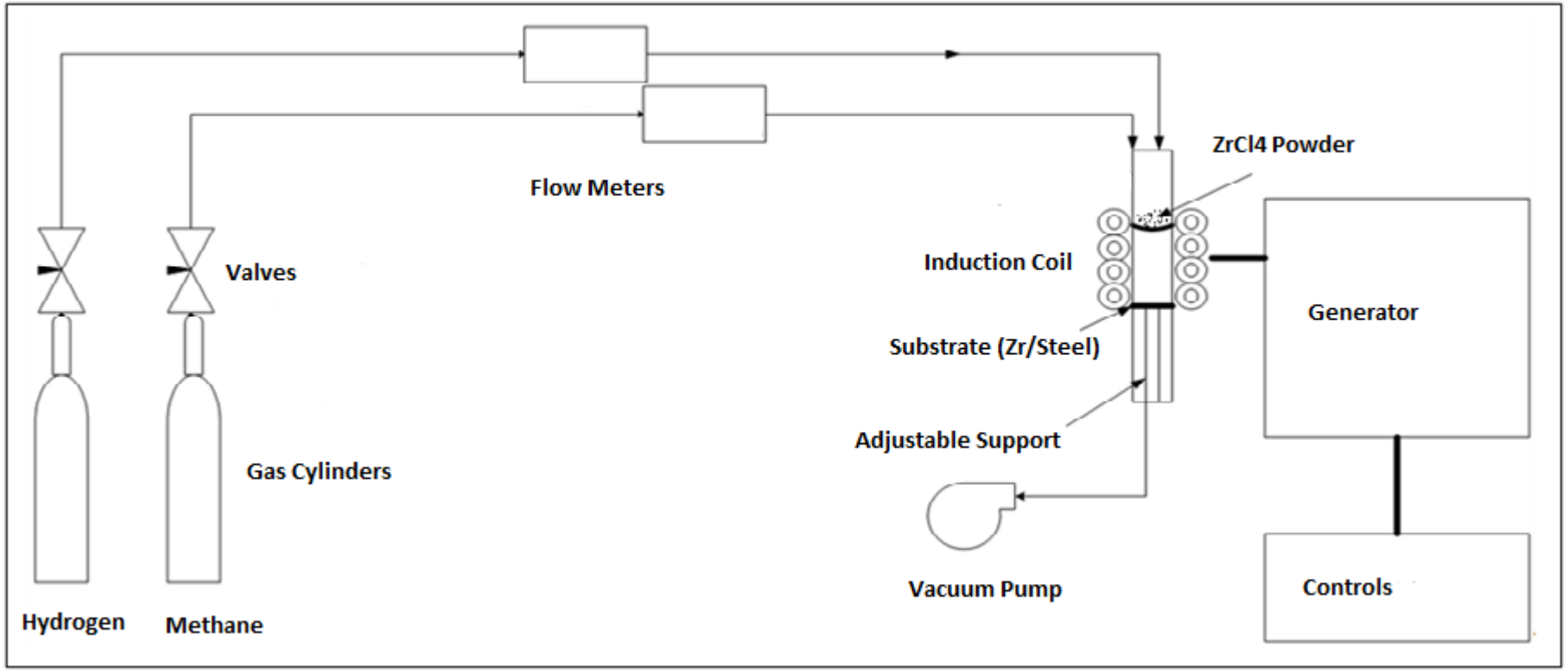


**Figure 9: Schematic diagram of experimental setup**

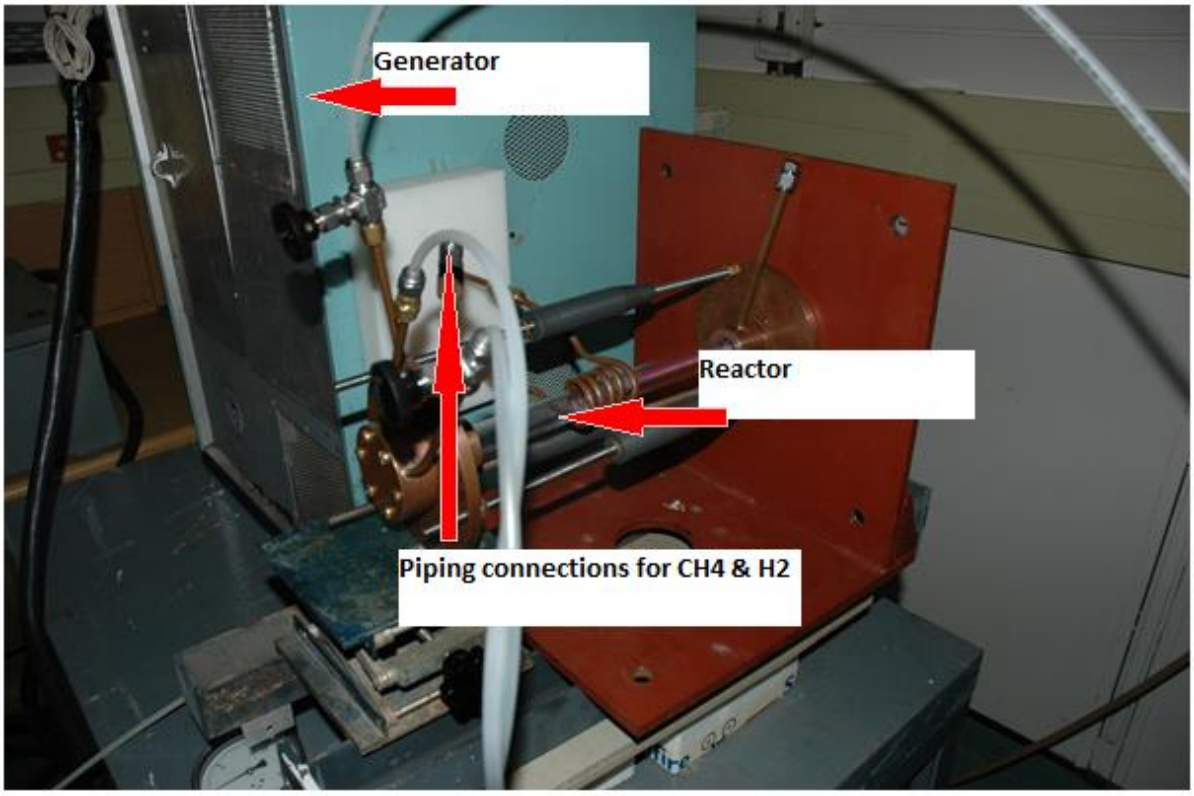


**Figure 10: Photographic representation of the connections in the experimental setup**

Figure 10 illustrates the photographic representation of connections in the experimental setup.

A stainless steel crucible was made to hold the $ZrCl_4$. The $ZrCl_4$ powder was used in the reactor in order to source Zr. The stainless steel substrate in the form of a plate was used initially for the determination of temperatures at different positions in the reactor. Later on, mild steel was used as substrate for the coating process of ZrC.

A copper coil was connected to the radio frequency (RF) generator, the RF generator was cooled by water and its power levels like voltage, current and grid current were adjusted through its control knobs. The reactor was mounted vertically inside the coil for the temperature determination and then placed horizontally for the coating process. Figure 9 shows the vertical position of the reactor for the initial temperature determination setup

using a pyrometer. The width of the induction section of the copper coil was 5.1 cm with five windings, through which water was circulated. The ends of the induction coils were connected to power supplies. Methane and hydrogen gases were admitted to the process system through the flow meters with control valves.

A scrubber was connected to the vacuum pump in order to remove the HCl vapour formed during the chemical reaction. The scrubber was filled with alumina spheres (Unisrob Mark 5) to absorb the vapours produced using the chemisorption technique.

Figure 11 also shows another view of the connections in the experimental setup specially depicting the generator and its controls.

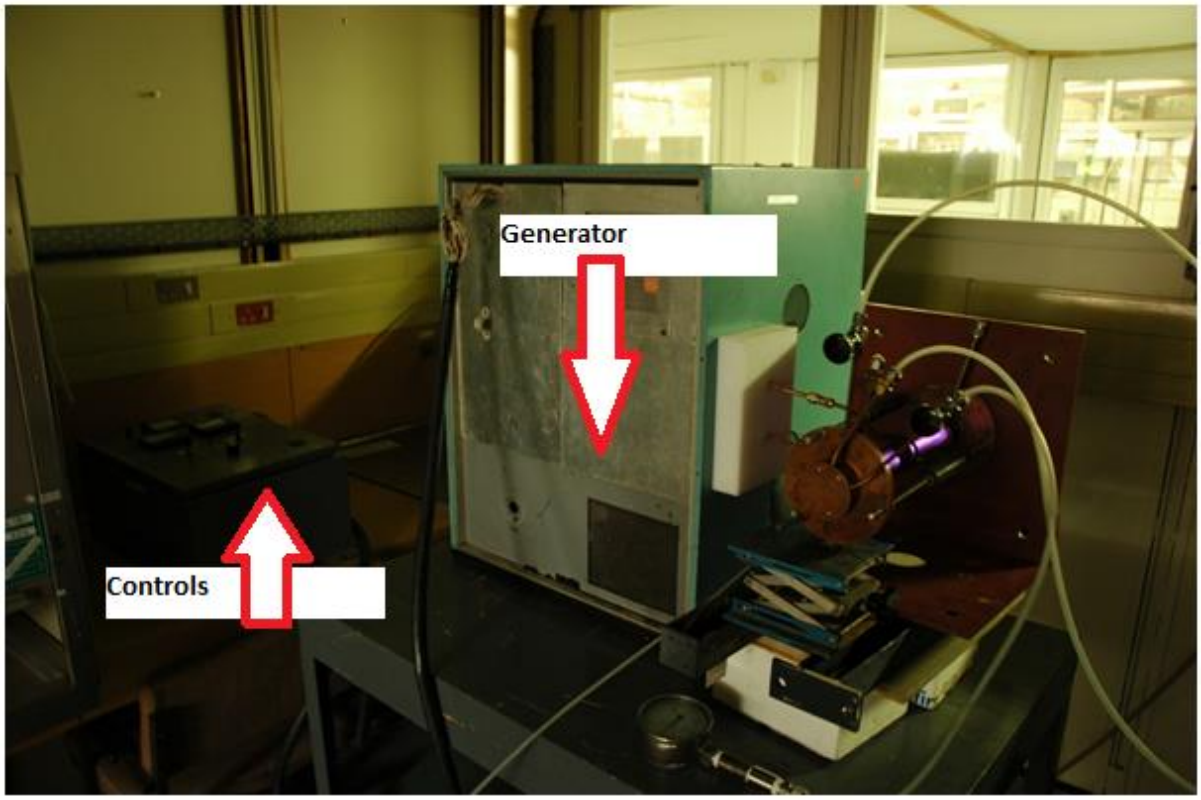


**Figure 11: Photographic representation of the experimental setup showing the generator and its controls**

## 3.2 Stoichiometry

Stoichiometric calculations were carried out according to chemical reaction **(5)** as shown below, to determine the quantities of the reactants that would be required and the equivalent amount of products that should be produced.

$$\mathbf{ZrCl_4 + CH_4 \rightarrow ZrC + 4HCl \qquad (5),}$$

$$233.04\ \text{g/mol} + 16.04\ \text{g/mol} \rightarrow 103.24\ \text{g/mol} + 145.84\ \text{g/mol}$$

The amount of $ZrCl_4$ used for reaction **(5)** was 2 g, since the size of the crucible can only accommodate that amount of $ZrCl_4$. The amount of ZrC should be produced according to reaction **(5)** (since the molar ratio of $ZrCl_4$ and ZrC is 1:1) = 0.008582 x 103.24 (See footnote[8]). The mass of ZrC = 0.8859 g

Similarly, for $CH_4$ gas, 0.008582 x 16.04 = 0.1377 g. Therefore, the volume of $CH_4$ gas = 0.22 l, would be required according to reaction **(5),** that was added continuously to the system.

The Gibbs free energy calculation of reaction **(5)** showed negative Δ G values, which indicates the possibility of that reaction to occur.

Table 3 shows the stoichiometric data of the reactants and products using reaction **(5)**.

[8] The number of moles of $ZrCl_4$ = 2 g/ (233.04) g/mol = 0.008582 moles. Density of methane = 0.6269 g/l

| Reactants/ Products | Molar Mass (g/mol) | No. of Moles | Mass (g) |
|---|---|---|---|
| $ZrCl_4$ | 233.04 | 0.008582 | 2 |
| $CH_4$ | 16.04 | 0.008582 | 0.1377 (0.22 l) |
| ZrC | 103.24 | 0.008582 | 0.8859 |
| HCl | 36.46 | 0.034328 | 1.2516 |

**Table 3: Determination of stoichiometric data of the reactants and products using chemical reaction (1)**

## 3.3 Temperature Calibration of the Reactor

It was important to determine the temperatures at different positions of the reactor to optimise the position for the coating, so that the crucible (that holds the $ZrCl_4$ powder) and mild steel substrate can be placed accurately at different positions inside the quartz tube (reactor). In order to determine the temperature at different positions, a steel plate supported with silica wool (Figure 12), was placed at various positions (X = 5 mm, 10 mm and 15 mm from the first turn of the coil) inside the quartz tube, heated by the induction coil and the temperature measured by means of a pyrometer. The temperature measured by the pyrometer at the first turn of the coil (X = 0) in the plasma condition was 661 $^{o}$C at a voltage reading of 1.2 kV.

The inside diameter of the reactor was 16 mm and the inside diameter of the coil was 40 mm. The reactor was placed in the centre of the coil 12 mm away from the coil. The height of the induction coil with 5 windings was 5.1 cm.

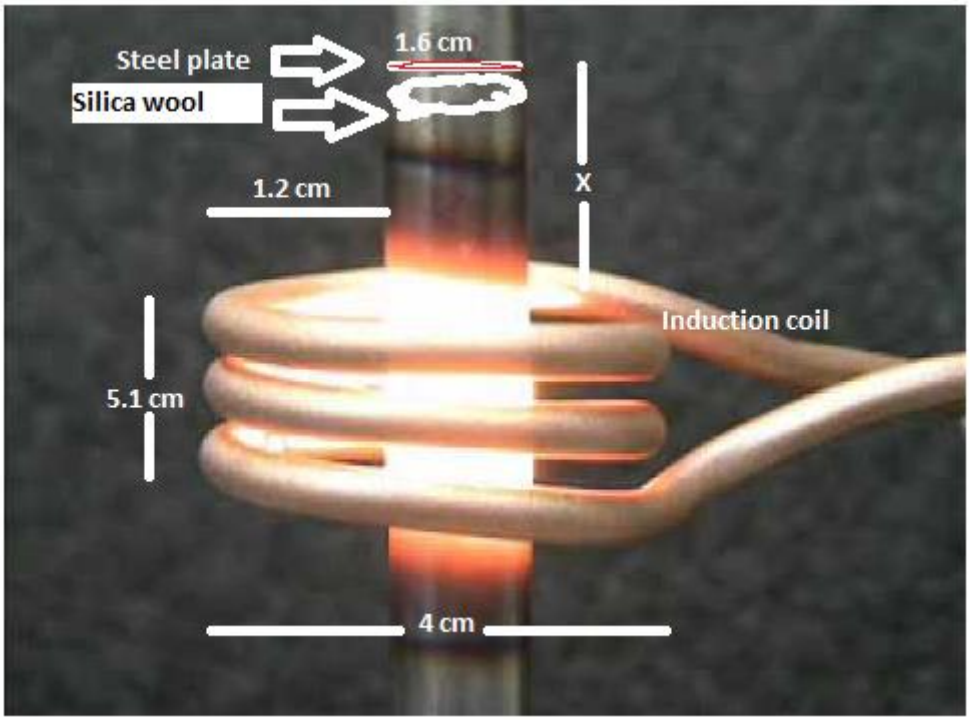


**Figure 12: Diagram showing temperature calibration setup of the reactor**

The emissivity of the steel plate was found by placing the steel plate in an oven heated to a temperature of 600 $^{o}$C. The pyrometer was used to determine the temperature of that and from the difference in temperatures the emissivity of the steel plate was calculated which was found to be 0.82.

Using the pyrometer, it was not possible to determine the temperature of the substrate if its temperature was below 500 $^{o}$C as the pyrometer used could only read a temperature up to 500 $^{o}$C, not below that temperature. Therefore, in order to determine temperatures of about 300 $^{o}$C inside the reactor at different positions, sodium nitrate ($NaNO_3$) was used as it has a melting point of 308 $^{o}$C. Sodium nitrate powder was placed inside the reactor at X = 5 mm, 10 mm and 15 mm above the top turn of the coil in the plasma condition. During this temperature measurement setup the reactor was mounted horizontally inside the induction

coil. Table 4 shows the temperatures at different heights of the reactor and at different voltages using the pyrometer and sodium nitrate.

| Voltage (kV) | Distance, X (mm) | Temperature ($^{o}$C) |
|---|---|---|
| 1.2 | 0 | 661 |
| 1.75 | 5 | > 308 |
| 2.5 | 10 | > 308 |
| 3 | 15 | > 308 |

**Table 4: Reactor tube temperature measurements data at different heights and at different voltages using the pyrometer and sodium nitrate**

The position at which $NaNO_3$ was melted showed that the temperature at this position is greater than 308 $^{o}$C with the corresponding applied voltage.

## 3.4 Substrate Preparation

The substrate used for the coating process by the cold plasma chemical vapour deposition technique was mild steel. It was polished with different grade silicon carbide (SiC) abrasive papers starting with coarse (120, 320 grit) and finally with fine grade (600, 1200 grit) paper. The substrate was subsequently washed with acetone and dried using an air dryer. The substrate was then weighed before it was placed at different positions inside the reactor. After the experiment the substrate collected from the reactor was labelled (see Table 5). Table 5 provides the narrative of the different substrates used, its positions in the reactor, exposure temperature and their reaction time for the plasma assisted chemical vapour deposition.

| Sample | Distance, X (mm) | Temperature($^{o}$C) | Weight (g) | Duration (minutes) |
|---|---|---|---|---|
| 1SUN30MS12 | 12 | > 308 | 9. 96 | 30 |
| 2SUN60MS14 | 14 | > 308 | 10.83 | 60 |
| 3SUN30MS8 | 8 | > 308 | 10.12 | 30 |
| 4SUN45MS10 | 10 | > 308 | 10.36 | 45 |

**Table 5: Substrate positions, weights and duration of the experiment**

## 3.5 Experimental Procedure

The experimental procedure for the plasma assisted chemical vapour deposition of the ZrC on the substrate was carried out as follows: The experimental setup as mentioned earlier (Figure 9) consisted of an RF generator (5 kW, 3 MHz), water cooled induction coil, a cylindrical quartz tube reactor, gas delivery system and off-gas exhaust system. The reactor consisted of a horizontally placed cylindrical quartz tube. Hydrogen ($H_2$) gas was used to initiate cold plasma (pinkish plasma) inside the quartz tube (reactor) at low pressures and then methane ($CH_4$) gas was introduced into the quartz tube (reactor), after that the colour of plasma changed to whitish. $CH_4$ was used as carbon source and hydrogen gas was admitted to displace the oxygen and to provide a reducing environment in order to ensure that the $CH_4$ did not combust on initiation of plasma.

The reactor was heated by the plasma for about 5 minutes in order to induce plasma stability. The $ZrCl_4$ powder in the crucible was then slowly introduced into the plasma. The transfer of $ZrCl_4$ powder from its bottle was done using the glove box as $ZrCl_4$ powder absorbs moisture from the atmosphere due to its hygroscopic nature.

Two modes of gas injection into the reactor were provided for the introduction of methane and hydrogen through a circular nozzle. The reaction time was between 30 minutes to 1 hour and the applied voltage was between 2 kV to 3 kV.

After the reaction process the plasma was quenched by reducing the applied voltage and by stopping the methane gas flow. The hydrogen gas supply was continued with reactor vessel closed in order to protect the products from getting oxidised at high temperatures, until the reactor system cooled down. The $ZrCl_4$ feed was 2 g and the flow rate of methane was 2 l/min. The flow rate of hydrogen was kept at a higher flow rate than the flow rate of methane. The formation of ZrC is an endothermic reaction.

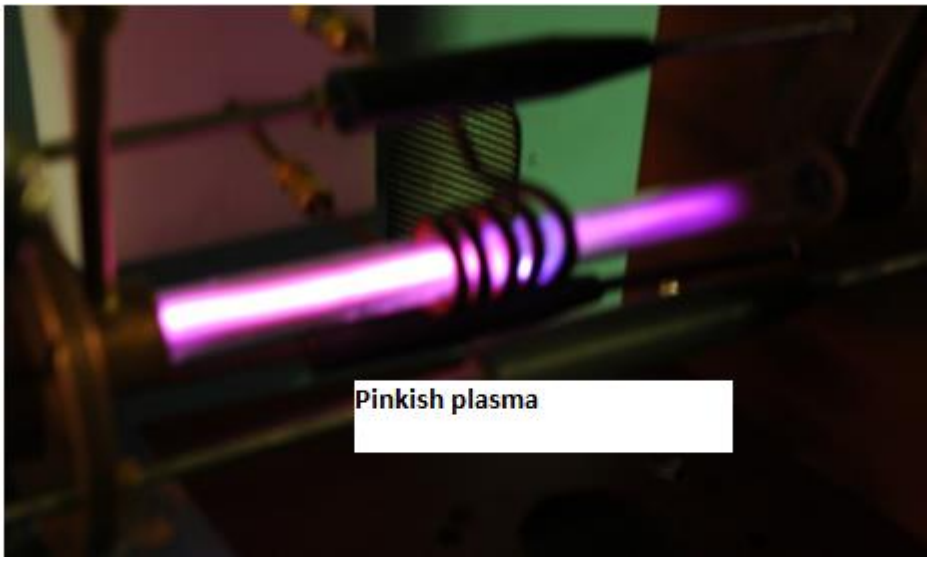


**Figure 13: A Photograph of the reactor tube showing the development of plasma in pinkish colour**

Figure 13 shows the development of plasma in a pink colour with the admission of only hydrogen gas flow into the system, when the methane gas was introduced into the reactor (see Figure 14 below) the colour of the plasma changed to whitish.

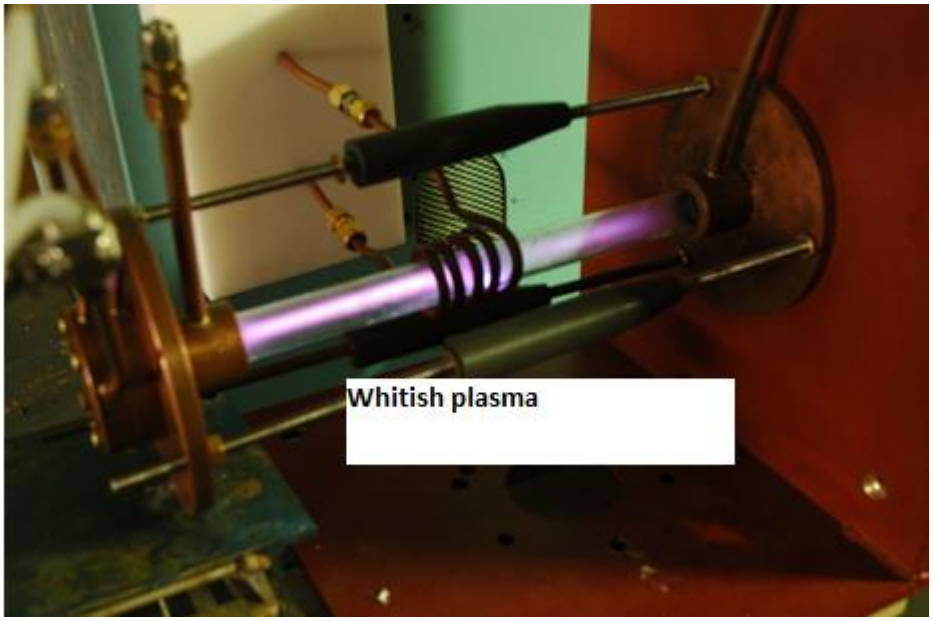


**Figure 14: A Photograph of the reactor tube showing the development of plasma in whitish colour**

Four samples were coated in this manner by varying the distance. These samples were then subjected to scanning electron microscopy (SEM) and X-ray Diffraction (XRD) to determine composition, microstructure and phases present. The characterization of the samples is discussed in Chapter 4.

# Chapter 4

# Results and Discussion

## 4.1 Sample 1SUN30MS12

Sample 1SUN30MS12 was coated using cold plasma assisted chemical vapour deposition coating technique and SEM analysis was carried out on the sample.

### 4.1.1. Scanning Electron Microscope (SEM) Results

The cross section morphology of the coatings was assessed using a SEM – FEI Quanta 200 D scanning electron microscope and for elemental analysis an EDAX Apollo X - SDD (Silicon Drifted Detector) was used. SEM provides useful information about the composition at the specimen surface. Figure 15 shows the scanning electron micrograph of sample 1SUN30MS12.

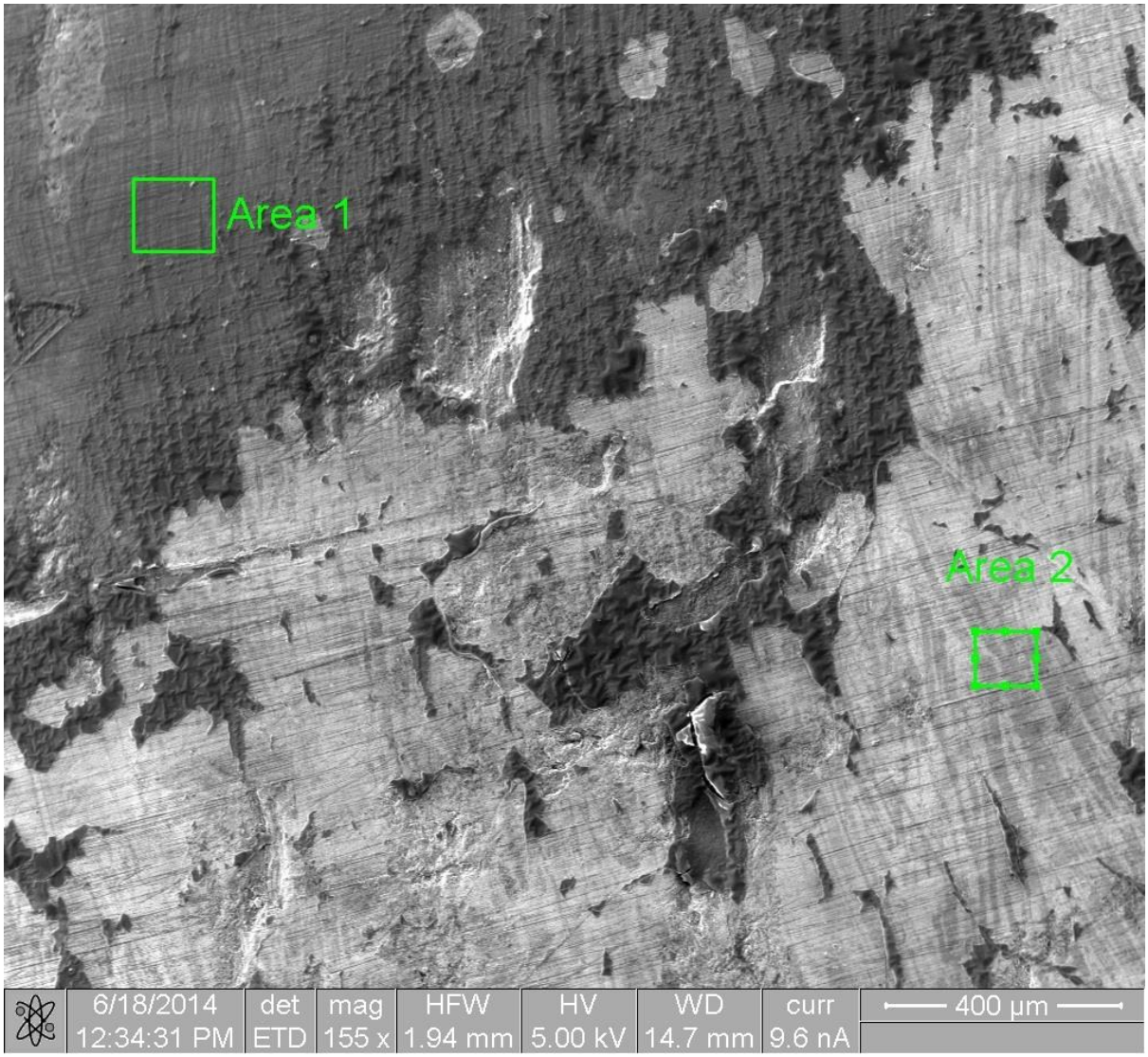


**Figure 15: SEM image of the coated sample 1SUN30MS12 showing marked Areas 1, 2 (highlighted in green)**

The two spectra shown in Figures 16 and 17 contain data obtained from Areas 1 and 2

respectively showing elements present.

## Area 1

kV: 5 Mag: 140 Takeoff: 39.2 Live Time(s): 30 Amp Time(µs): 12.8 Resolution:(eV)129.4

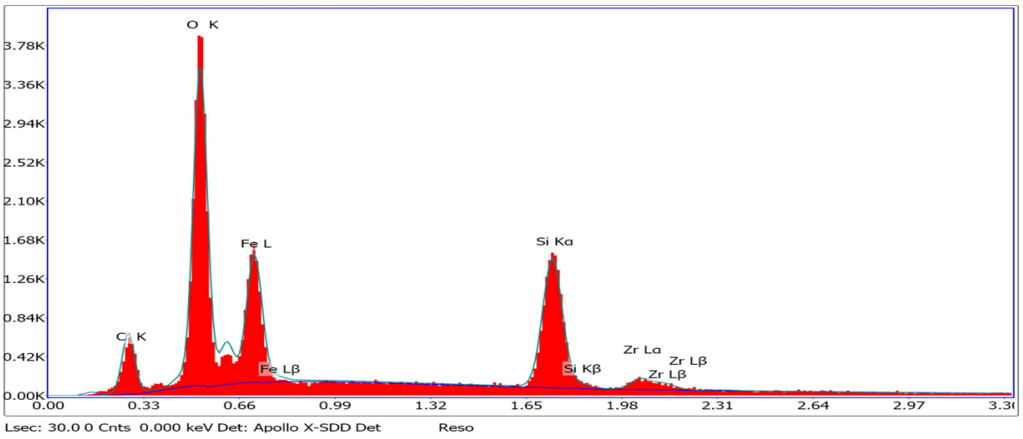


| Element | Weight % | Atomic % |
|---|---|---|
| C K | 9.54 | 18.64 |
| O K | 31.05 | 45.56 |
| FeL | 21.66 | 9.1 |
| SiK | 29.36 | 24.54 |
| ZrL | 8.39 | 2.16 |

**Figure 16: SEM spectrum and the associated data of Area 1 of sample 1SUN30MS12.**

X-Ray fluorescence spectrum (Figure 16) of Area 1 showing the determined weight and atomic percentages of elements detected. The spectrum shows the elemental presence of carbon (C), oxygen (O), iron (Fe), silicon (Si) and zirconium (Zr).

## Area 2

kV: 5 Mag: 140 Takeoff: 39.2 Live Time(s): 30 Amp Time(µs): 12.8 Resolution:(eV)129.4

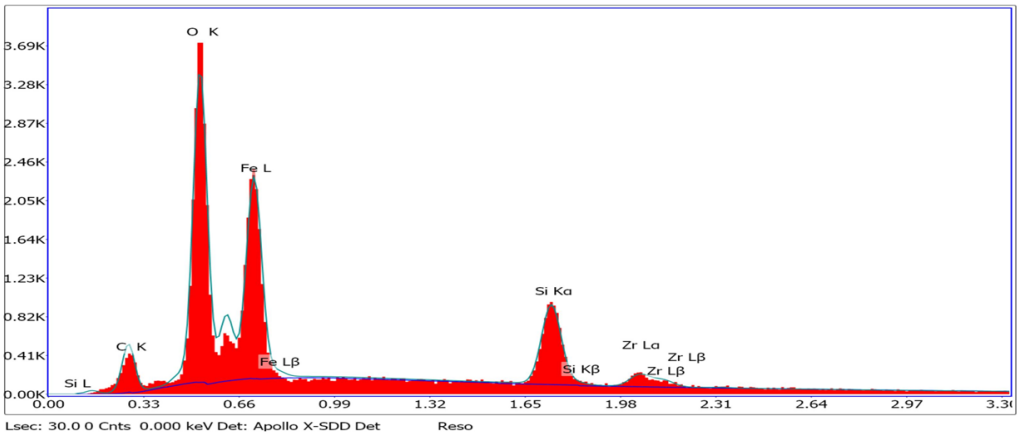


| Element | Weight % | Atomic % |
|---|---|---|
| C K | 7.31 | 15.77 |
| O K | 29.79 | 48.22 |
| FeL | 34.77 | 16.13 |
| SiK | 18.65 | 17.2 |
| ZrL | 9.48 | 2.69 |

**Figure 17: SEM spectrum and the associated data of Area 2 of sample 1SUN30MS12.**

X-ray fluorescence spectrum (Figure 17) of Area 2 showing the determined weight and atomic percentages of elements detected. The spectrum shows the elemental presence of carbon (C), oxygen (O), iron (Fe), silicon (Si) and zirconium (Zr). The other samples also gave similar results, but only differed in the amounts of elements.

## 4.2 X-ray Diffraction Results

In order to determine the phases present in the coating, the samples were subjected to X-ray Diffraction analysis. For comparison purposes a ZrC powder standard (ICDD) was also analyzed. The diffractograms obtained of the samples were compared with the diffractograms of the standard (the peak positions of diffractograms were compared). The characterization of the four samples and ZrC powder was studied by using X-ray Diffraction in a PANalytical X'Pert Pro diffractometer instrument that is equipped with a 2 theta goniometer stage, highly collimated Cu Kα, incident X-ray beam with a beam size of 0.8 mm in diameter and an area detector system and used ICDD PDF 4+ version 2015 to do the identifications of the samples. XRD patterns and the data of the samples are presented below along with the pattern and data for ZrC which is used as a standard.

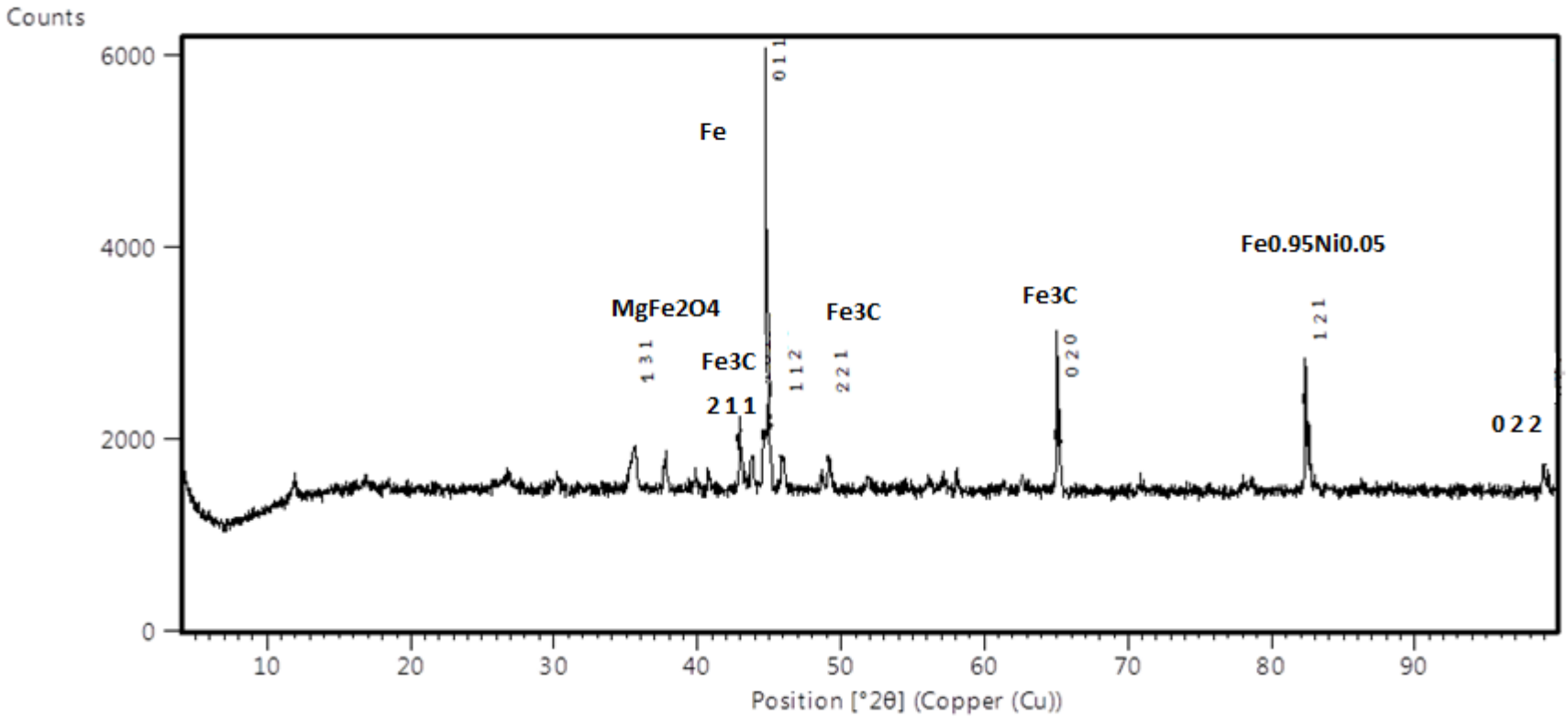


**Figure 18: XRD pattern of sample 1SUN30MS12 indicating hkl values and some identified peaks**

The 2 theta, d-spacing, intensity, hkl values and identified compound of sample 1SUN30MS12 are given in Table 6. This sample contains peaks from magnesium iron oxide ($MgFe_2O_4$), iron carbide ($Fe_3C$), iron (Fe) and iron nickel ($Fe_{0.95}Ni_{0.05}$) [36].

| Pos. [°2θ] | d-spacing [Å] | Intensity [%] | H | k | l | Compound |
|---|---|---|---|---|---|---|
| 35.5237 | 2.52506 | 12.56 | 1 | 3 | 1 | Magnesium iron oxide |
| 42.9628 | 2.1035 | 12.20 | 2 | 1 | 1 | Iron carbide |
| 43.8157 | 2.06451 | 11.72 | 1 | 0 | 2 | Iron carbide |
| 44.591 | 2.0304 | 15.08 | 2 | 2 | 0 | Iron carbide |
| 44.739 | 2.02403 | 100 | 0 | 1 | 1 | Iron |
| 44.878 | 2.01808 | 20.05 | 0 | 3 | 1 | Iron carbide |
| 45.9199 | 1.97468 | 9.19 | 1 | 1 | 2 | Iron carbide |
| 49.1506 | 1.85218 | 8.99 | 2 | 2 | 1 | Iron carbide |
| 65.1132 | 1.43143 | 13.60 | 0 | 2 | 0 | Iron carbide |
| 82.4507 | 1.16885 | 24.26 | 1 | 2 | 1 | Iron nickel |
| 99.0931 | 1.01231 | 7.78 | 0 | 2 | 2 | Iron nickel |

**Table 6: The 2 theta, d-spacing, intensity hkl values and identified compound of sample 1SUN30MS12**

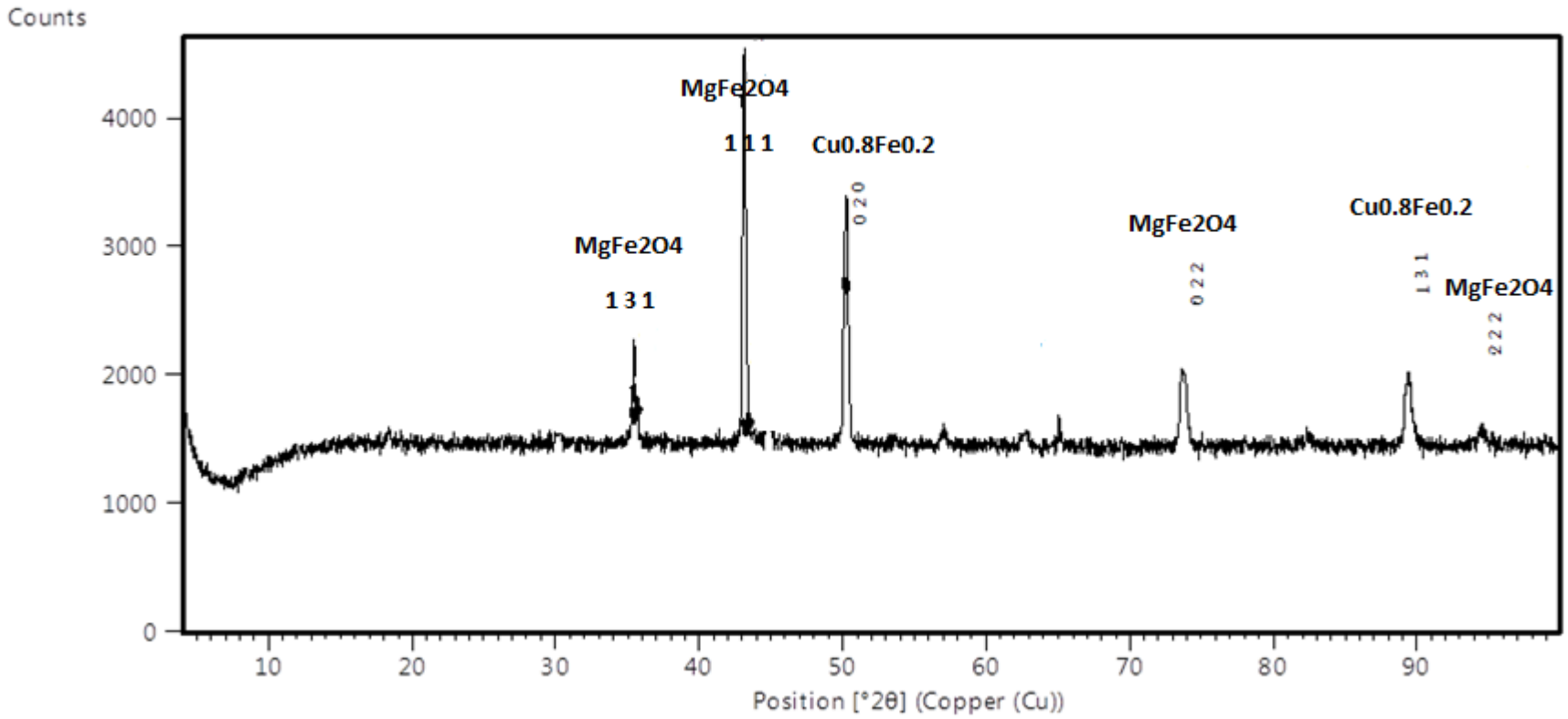


**Figure 19: XRD pattern of sample 2SUN60MS14 indicating hkl values and identified peaks**

The d-spacing, 2 theta, intensity, hkl values and identified compound of sample 2SUN60MS14 are given in Table 7. This sample contains peaks from magnesium iron oxide ($MgFe_2O_4$) and copper iron ($Cu_{0.8}Fe_{0.2}$) [36].

| Pos. [°2θ] | d-spacing [Å] | Intensity [%] | h | k | l | Compound |
|---|---|---|---|---|---|---|
| 35.5492 | 2.52331 | 12.69 | 1 | 3 | 1 | Magnesium iron oxide |
| 43.1079 | 2.09675 | 100.0 | 1 | 1 | 1 | Magnesium iron oxide |
| 50.1972 | 1.81598 | 45.36 | 0 | 2 | 0 | Copper iron |
| 73.7084 | 1.2843 | 22.86 | 0 | 2 | 2 | Magnesium iron oxide |
| 89.3783 | 1.09533 | 24.70 | 1 | 3 | 1 | Copper iron |
| 94.5331 | 1.04871 | 7.17 | 2 | 2 | 2 | Magnesium iron oxide |

**Table 7: The 2 theta, d-spacing, intensity, hkl values and identified compound of sample 2SUN60MS14**

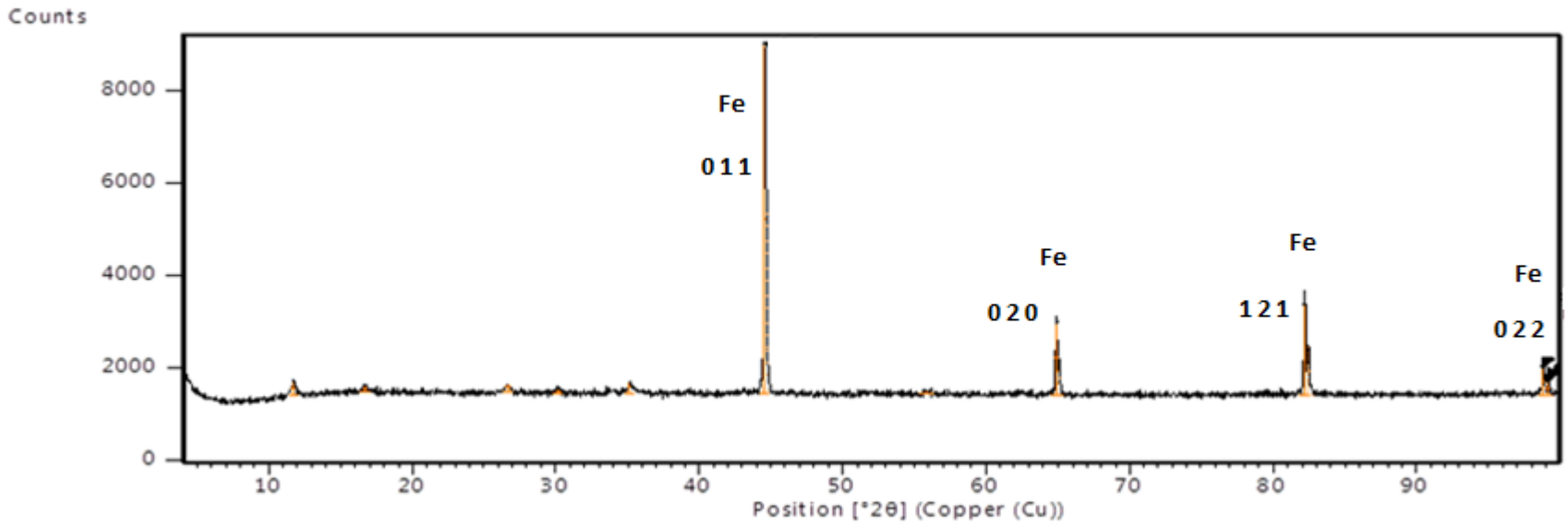


**Figure 20: XRD pattern of sample 3SUN30MS8 indicating hkl values and identified peaks**

The d-spacing, 2 theta, intensity, hkl values and identified compound of sample 3SUN30MS8 are given in Table 8. This sample contains peaks from iron (Fe) only [36].

| Pos. [°2θ] | d-spacing [Å] | Intensity [%] | h | k | l | Compound |
|---|---|---|---|---|---|---|
| 44.5613 | 2.03168 | 100.0 | 0 | 1 | 1 | Iron |
| 64.9081 | 1.43546 | 13.61 | 0 | 2 | 0 | Iron |
| 82.2174 | 1.17158 | 24.31 | 1 | 2 | 1 | Iron |
| 98.8235 | 1.01435 | 7.79 | 0 | 2 | 2 | Iron |

**Table 8: The 2 theta, d-spacing, intensity, hkl values and identified compound of sample 3SUN30MS8**

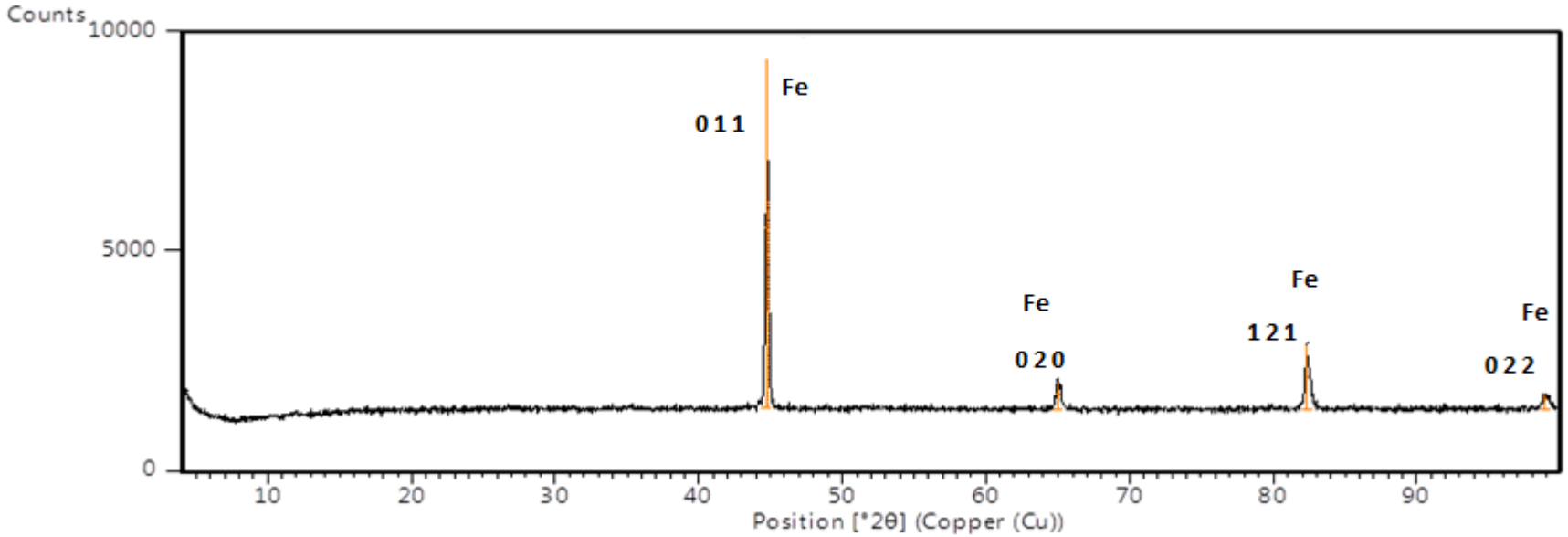


**Figure 21: XRD pattern of sample 4SUN45MS10 indicating hkl values and identified peaks**

The 2 theta, d-spacing, intensity, hkl values and identified compound of sample 4SUN45MS10 are given in Table 9. This sample contains peaks from iron (Fe) only [36].

| Pos. [°2θ] | d-spacing [Å] | Intensity [%] | h | k | l | Compound |
|---|---|---|---|---|---|---|
| 44.7087 | 2.02533 | 100.0 | 0 | 1 | 1 | Iron |
| 65.047 | 1.43273 | 13.65 | 0 | 2 | 0 | Iron |
| 82.3467 | 1.17006 | 24.43 | 1 | 2 | 1 | Iron |
| 98.9424 | 1.01345 | 7.85 | 0 | 2 | 2 | Iron |

**Table 9: The 2 theta, d-spacing, intensity, hkl values and identified compound of sample 4SUN45MS10**

The XRD spectrum of ZrC powder that was analysed in the laboratory is given in Figure 22.

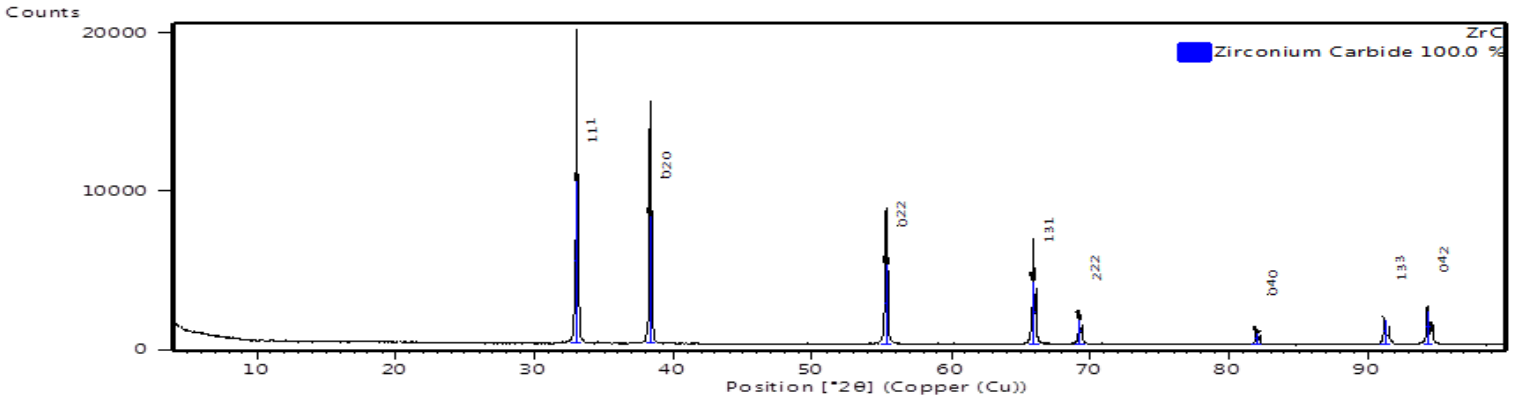


**Figure 22: XRD pattern of ZrC indicating hkl values**

The d-spacing, 2 theta, intensity and hkl values of the standard ZrC are given in Table 10.

| Pos. [°2θ] | d-spacing [Å] | Intensity [%] | h | k | l | Compound |
|---|---|---|---|---|---|---|
| 33.0381 | 2.70914 | 100 | 1 | 1 | 1 | ZrC |
| 38.3255 | 2.34666 | 78.32 | 0 | 2 | 0 | ZrC |
| 55.2948 | 1.66002 | 48.96 | 0 | 2 | 2 | ZrC |
| 65.9176 | 1.4159 | 38.58 | 1 | 3 | 1 | ZrC |
| 69.2501 | 1.35567 | 15.50 | 2 | 2 | 2 | ZrC |
| 81.9941 | 1.1742 | 7.05 | 0 | 4 | 0 | ZrC |
| 91.2584 | 1.0776 | 15.98 | 1 | 3 | 3 | ZrC |
| 94.3416 | 1.05034 | 20.90 | 0 | 4 | 2 | ZrC |

**Table 10: The 2 theta, d-spacing, intensity and hkl values of ZrC**

XRD patterns of the 4 samples are shown below together with the spectrum of ZrC used as a standard.

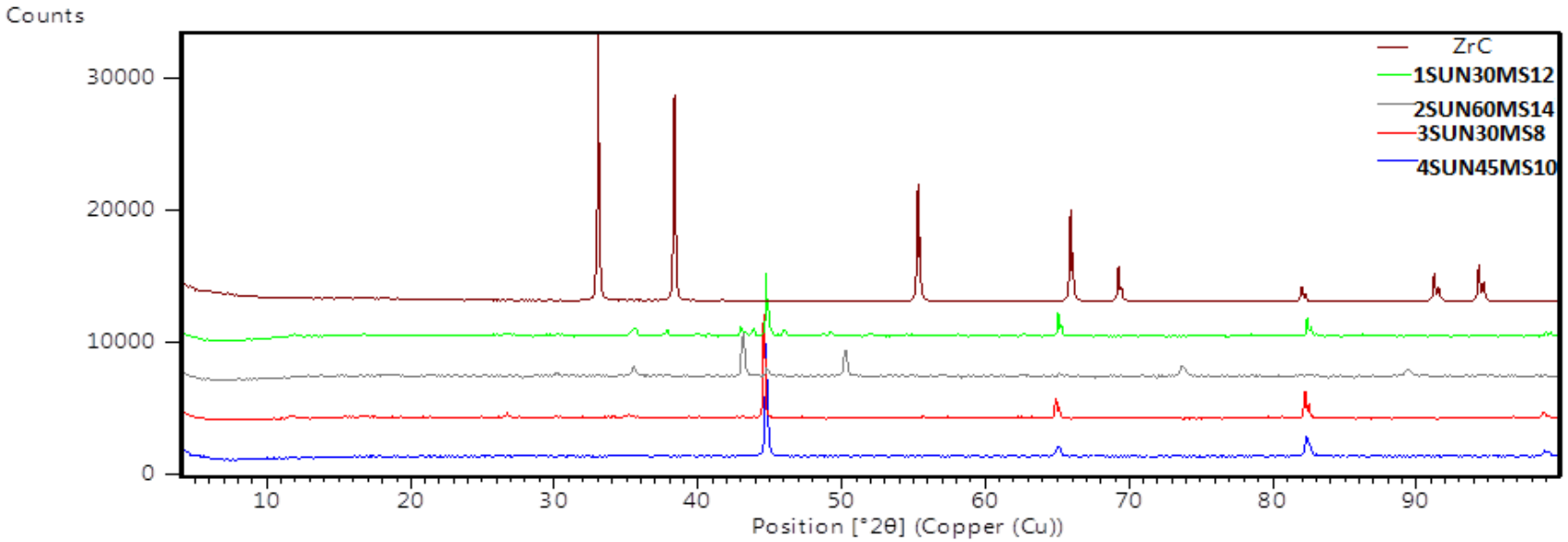


**Figure 23: XRD patterns of 4 samples and the pattern for ZrC powder used as a standard**

## 4.3 Discussion

Scanning Electron Microscope (SEM) and X-ray Diffraction results are discussed below. SEM results showed the presence of carbon (C), iron (Fe), oxygen (O), silicon (Si) and zirconium (Zr) in the samples. The elemental presence of carbon is from the methane gas and mild steel substrate, iron from the mild steel, oxygen from the atmosphere through the reactor connection leak, silicon from the grease used as a sealant at the connection point of the reactor quartz tube and also from mild steel and zirconium from the $ZrCl_4$.

X-ray Diffraction analysis conducted on the samples exhibited the compounds present in the samples. The peaks of the diffractograms of the samples were identified by comparing with the standard ZrC powder (ICDD).

The sample 1SUN30MS12 contained peaks from magnesium iron oxide ($MgFe_2O_4$), iron carbide ($Fe_3C$), iron (Fe) and iron nickel ($Fe_{0.95}Ni_{0.05}$), see Table 6. The sample 2SUN60MS14 contained peaks from magnesium iron oxide ($MgFe_2O_4$) and copper iron ($Cu_{0.8}Fe_{0.2}$), see Table 7. The remaining two samples contained peaks from only iron, see Table 8 &9.

Figure 23 showed the comparison of the peaks from the 4 samples with the peaks of the ZrC powder which is used as a reference. The aim of this experiment was to produce ZrC and to coat the substrate with the ZrC. From the XRD results it can be established that ZrC was not coated on the surface of the substrate, even though SEM results showed the presence of Zr and C.

The next chapter (Chapter 5) discusses the conclusion from the results obtained.

# Chapter 5

# Conclusion

## 5.1 Conclusion

The mechanical properties and low neutron absorption of zirconium alloys have attributed to their wide use as fuel cladding materials in Light Water Reactors (LWRs). The lack of corrosion resistance is one of the key life-limiting phenomena of zirconium alloy cladding which has resulted in the need to find ways of addressing the problem by use of coatings, such as, silicon carbide (SiC) and zirconium carbide (ZrC).

The focus of this study was to scrutinize available literature on deposition of ZrC using various coating methods with the aim of finding and applying a feasible method to coat ZrC on nuclear fuel rods, that is cost effective and high in deposition rate.

Literature study [4] [11] [22] [24] showed that CVD was used for application in nuclear fuel, as well as the manufacture of nuclear ceramics used in nuclear reactors. Subsequently, the approach used was a modified method such as a plasma assisted chemical vapour deposition process, that is well suited for coating Zr alloy fuel rods with ZrC for nuclear applications.

In this study, a Radio Frequency (RF) cold plasma assisted chemical vapour deposition method using a set of parameters such as low temperature, distance (X) of the substrate, flow rates of methane and hydrogen gas and low pressure was used. Scanning Electron Microscopy (SEM) and X-ray Diffraction (XRD) have been used to characterize the samples. The results of SEM showed the presence of Zr and C in the samples. However, the XRD results did not confirm the presence of ZrC as a compound. Therefore, further work is necessary to determine the suitable parameters for the ZrC production using the plasma assisted chemical vapour deposition method. However, if the experimental results had

indicated the presence of ZrC coating on mild steel substrate, then the experiment would have been repeated using Zr alloy as substrate.

ZrC coating was not obtained on the substrate, possibly due to the following factors:

- insufficient vacuum
- leaks through the connectors of the reactor used
- inability to maintain the minimum required temperature in the reactor, as well as, the improper position of substrate and
- difficulty in optimising the accurate flow rates of methane and hydrogen gases.

Following these challenges, it is recommended that, further studies be considered using acetylene instead of methane gas to supply more carbon. Furthermore, the design of the reactor should be leak tight and the gas flow rates and temperatures be optimized.

# References

1) L. Hallstadius, S. Johnson and E. Laholda. 2012. Cladding for high performance fuel. Progress in Nuclear Energy. 57: 71-76.

2) M. Steinbrück and M. Böttcher. 2012. Air oxidation of Zircaloy-4, M5® and ZIRLO™ cladding alloys at high temperatures. Journal of Nuclear Materials. 421: 160-171.

3) V. Craciun, E. J. McCumiskey, M. Hanna and C. R. Taylor. 2013. Very hard ZrC thin films grown by pulsed laser deposition. Journal of the European Ceramic Society. 33: 2223-2226.

4) L. Zhu, N. Zhang, B. Zhang, F. Sun, R. Bolot, M. P. Planche, H. Liao, C. Coddet. 2011. Very low pressure plasma sprayed alumina and yttria-stabilized zirconia thin dense coatings using a modified transferred arc plasma torch. Applied Surface Science. 258: 1422-1428.

5) G. Vasudevamurthy, T. W. Knight, E. Roberts and T. M. Adams. 2008. Laboratory production of zirconium carbide compacts for use in inert matrix fuels. Journal of Nuclear Materials. 374: 241-247.

6) D. Craciun, G. Socol, N. Stefan, I. N. Mihailescu, G. Bourne and V. Craciun. 2009. High-repetition rate pulsed laser deposition of ZrC thin films. Surface and Coatings Technology. 203: 1055-1058.

7) S. C. Velasco, V. Lopez, C. F. Almeida Alves, A. Cavaleiro and S. Carvalho. 2014. Structural and electrochemical characterization of Zr-C-N-Ag coatings deposited by DC dual magnetron sputtering. Corrosion Science. 80: 229-236.

8) T. S. Sidhu, S. Prakash and R. D. Agrawal. 2005. Studies on the properties of high-velocity oxy-fuel thermal spray coatings for higher temperature applications. Materials Science. 41(6): 805-823.

9) Y. Xin, S. Zhe-an, H. Qi-zhong, C. Li-yuan, Z. Ping and X. Liang. 2014. A zirconium carbide coating on graphite prepared by reactive melt infiltration. J. Cent. South Univ. 21: 472-476.

10) Nuclear Corrosion Science and Engineering, edited by Damien Feron, Woodhead Publishing Limited, 2012.

11) D. Lu, Y. Niu, X. Ge, X. Zheng and G. Chen. 2014. Fabrication and Ablation Behavior of Plasma Sprayed ZrC-W Composite Coatings. Key Engineering Materials Vols. 602-603: 552-555.

12) Y. S. Nam, X. M. Cui, L. Jeong, J. Y. Lee and W. H. Park. 2009. Fabrication and characterization of zirconium carbide (ZrC) nanofibers with thermal storage property. Thin Solid Films. 517: 6531-6538.

13) Y. Katoh, G. Vasudevamurthy, T. Nozawa and L.L. Snead. 2013. Properties of zirconium carbide for nuclear fuel applications. Journal of Nuclear Materials. 441: 718-742.

14) L. B. Zuev, S. Y. Zavodchikov, T. M. Poletika, G. S. Cheremnykh, V. B. Filippov, V. I. Belov, V. M. Arzhakova, O. V. Bocharov and A. K. Shikov. 2005. Phase Composition, Structure and Plastic Deformation Localization in Zr 1% Nb alloys. ASTM, STP 1467-EB.

15) S. Abolhassani, R. Restani, T. Rebac, F. Groeschel, W. Hoffelner, G. Bart, W. Goll and F. Aeschbach. 2005. TEM Examinations of the Metal-Oxide Interface of Zirconium Based Alloys Irradiated in a Pressurized Water Reactor. Journal of ASTM International. 2(6): 467-492.

16) H. K. Yueh, R. L. Kesterson, R. J. Comstock, H. H. Shah, D. J. Colburn, M. Dahlback, and L. Hallstadius. 2005. Improved ZIRLO$^{TM}$ Cladding Performance through Chemistry and Process Modifications. Journal of ASTM International. 2(6): 330-346.

17) Y. Long, A. Javed, J. Chen, Z. Chen and X. Xiong. 2014. Phase composition, microstructure and mechanical properties of ZrC coatings produced by chemical vapour deposition. Ceramics International. 40: 707-713.

18) J. Singh and D. E Wolfe. 2005. Review. Nano and macro-structured component fabrication by electron beam-physical vapour deposition (EB-PVD). Journal of Materials Science. 40: 1-26.

19) Kai Wang. 2013. Laser Based Fabrication of Graphene. “Advances in Graphene Science” ISBN 978-953-51-1182-5. Chapter 4.

20) V. A. Frolova, V. A. Poklad, B. V. Ryabenko, D. L. Kozlov and A. V. Zimareva. 2011. Spraying of coatings with the supply of aqueous solutions of various compounds into the plasma jet. Welding International. 25(3): 244-247.

21) Y. Bai, F. L. Yu, S. W. Lee, H. Chen and J. F. Yang. 2012. Characterization of the Near-Eutectic $Al_2O_3$–40 wt % $ZrO_2$ Composite Coating Fabricated by Atmospheric Plasma Spray. Materials and Manufacturing Processes. 27: 58-64.

22) G. Mauer, A. Hospach and R. Vaßen. 2013. Process development and coating characteristics of plasma spray-PVD. Surface and Coatings Technology. 220: 219-224.

23) D. Craciun, G. Socol, N. Stefan, G. Bourne, V. Craciun. 2009. Chemical composition of ZrC thin films grown by pulsed laser deposition. Applied Surface Science. 255 (10): 5260-5263.

24) D. Matejka and B. Benko. 1989. Plasma spraying of metallic and ceramic materials. Czechoslovakia, John Wiley & Sons Ltd.

25) A. F. Guillermet. 1995. Analysis of thermochemical properties and phase stability in the zirconium-carbon system. Journal of Alloys and Compounds. 217: 69 – 89.

26) H. F. Jackson, D. D. Jayaseelan, D. Manara, C. P. Casoni and W. E. Lee. 2011. Laser Melting of Zirconium Carbide: Determination of Phase Transitions in Refractory Ceramic Systems. Journal of the American Ceramic Society. 94 (10): 3561 – 3569.

27) E.K. Storms. 1967. The Refractory Carbides. Vol. 2. New York: Academic Press.

28) X. G. Wang, W. M. Guo, Y. M. Kan, G. J. Zhang, P. L. Wang. 2011. Densification behaviour and properties of hot-pressed ZrC ceramics with Zr and graphite additives. Journal of the European Ceramic Society. 31: 1103–1111.

29) C. Nachiappan, L. Rangaraj, C. Divakar, V. Jayaram. 2010. Synthesis and densification of monolithic zirconium carbide by reactive hot pressing, Journal of the American Ceramic Society. 93:1341–1346.

30) M. Balaceanu, M. Braic, V. Braic, A. Vladescu, C. C. Negrila. 2005. Surface chemistry of plasma deposited ZrC hard coatings, Journal of Opto electronics and Advanced Materials. 7: 2557–2560.

31) Y. Wang, Q. Liu, J. Liu, L. Zhang, L. Cheng. 2008. Deposition Mechanism for Chemical Vapour Deposition of Zirconium Carbide Coatings. Journal of the American Ceramic Society. 91 (4): 1249-1252.

32) I. J. van der Walt, J. T. Nel, J. L. Havenga. 2015. Plasma technology for the manufacturing of nuclear materials at Necsa. Journal of the Southern African Institute of Mining and Metallurgy. ISSN 2411-9717.

33) J. Singh, D. E. Wolfe, R. A. Miller, J. I. Eldridge, Dong-Ming Zhu. 2004. Tailored microstructure of zirconia and hafnia-based thermal barrier coatings with low thermal conductivity and high hemispherical reflectance by EB-PVD. Journal of Materials Science. 39 (6): 1975-1985.

34) H. M. Abourayana and D. P. Dowling. 2015. Plasma Processing for Tailoring the Surface Properties of Polymers. Chapter 5, ISBN 978-953-51-2216-6.

35) O. A Hamadi. 2008. The Fundamentals of Plasma-Assisted CVD Technique Employed in Thin Films Production. Iraqi Journal of Applied Physics Letters. Vol 1, No. 2.

36) International Centre for Diffraction Data, PDF 4+ Version, 2015.